UNIVERSITY OF AMSTERDAM

UvA-DARE (Digital Academic Repository)

# Phosphoproteome and drug-response effects mediated by the three protein phosphatase 2A inhibitor proteins CIP2A, SET, and PME-1

Kauko, Otto; Imanishi, Susumu Y.; Kulesskiy, Evgeny; Yetukuri, Laxman; Laajala, Teemu Daniel; Sharma, Mukund; Pavic, Karolina; Aakula, Anna; Rupp, Christian; Jumppanen, Mikael; Haapaniemi, Pekka; Ruan, Luyao; Yadav, Bhagwan; Suni, Veronika; Varila, Taru; Corthals, Garry L.; Reimand, Jüri; Wennerberg, Krister; Aittokallio, Tero; Westermarck, Jukka

**DOI**
10.1074/jbc.RA119.011265

**Publication date**
2020

**Document Version**
Final published version

**Published in**
Journal of Biological Chemistry

**License**
CC BY

Link to publication

**Citation for published version (APA):**
Kauko, O., Imanishi, S. Y., Kulesskiy, E., Yetukuri, L., Laajala, T. D., Sharma, M., Pavic, K., Aakula, A., Rupp, C., Jumppanen, M., Haapaniemi, P., Ruan, L., Yadav, B., Suni, V., Varila, T., Corthals, G. L., Reimand, J., Wennerberg, K., Aittokallio, T., & Westermarck, J. (2020). Phosphoproteome and drug-response effects mediated by the three protein phosphatase 2A inhibitor proteins CIP2A, SET, and PME-1. *Journal of Biological Chemistry*, *295*(13), 4194-4211. https://doi.org/10.1074/jbc.RA119.011265

**General rights**
It is not permitted to download or to forward/distribute the text or part of it without the consent of the author(s) and/or copyright holder(s), other than for strictly personal, individual use, unless the work is under an open content license (like Creative Commons).

**Disclaimer/Complaints regulations**
If you believe that digital publication of certain material infringes any of your rights or (privacy) interests, please let the Library know, stating your reasons. In case of a legitimate complaint, the Library will make the material inaccessible and/or remove it from the website. Please Ask the Library: https://uba.uva.nl/en/contact, or a letter to: Library of the University of Amsterdam, Secretariat, P.O. Box 19185, 1000 GD Amsterdam, The Netherlands. You will be contacted as soon as possible.

*UvA-DARE is a service provided by the library of the University of Amsterdam (https://dare.uva.nl)*

Download date:05 Sep 2026

# Phosphoproteome and drug-response effects mediated by the three protein phosphatase 2A inhibitor proteins CIP2A, SET, and PME-1

Received for publication, September 29, 2019, and in revised form, February 3, 2020 Published, Papers in Press, February 18, 2020, DOI 10.1074/jbc.RA119.011265

**Otto Kauko[‡§¶1], Susumu Y. Imanishi[‡2], Evgeny Kulesskiy[‖], Laxman Yetukuri[‡], Teemu Daniel Laajala[‖**], Mukund Sharma[‡§¶], Karolina Pavic[‡], Anna Aakula[‡], Christian Rupp[‡], Mikael Jumppanen[‡], Pekka Haapaniemi[‡], Luyao Ruan[‡‡], Bhagwan Yadav[‖], Veronika Suni[‡], Taru Varila[‡], Garry L. Corthals[‡], Jüri Reimand[‡‡§§], Krister Wennerberg[‖3], Tero Aittokallio[‖**], and Jukka Westermarck[‡§4]**

*From the [‡]Turku Bioscience Centre, University of Turku and Åbo Akademi University, 20500 Turku, Finland, the [§]Institute of Biomedicine, University of Turku, 20500 Turku, Finland, the [¶]TuBS and TuDMM Doctoral Programmes, University of Turku, 20500 Turku, Finland, the [‖]Institute for Molecular Medicine Finland FIMM, University of Helsinki, Tukholmankatu 8, Helsinki, Finland, the [**]Department of Mathematics and Statistics, University of Turku, 20500 Turku, Finland, the [‡‡]Computational Biology Program, Ontario Institute for Cancer Research, Toronto, Ontario M5G 0A3, Canada, and the [§§]Department of Medical Biophysics, University of Toronto, Toronto, Ontario M5G 1L7, Canada*

Edited by Roger J. Colbran

**Protein phosphatase 2A (PP2A) critically regulates cell signaling and is a human tumor suppressor. PP2A complexes are modulated by proteins such as cancerous inhibitor of protein phosphatase 2A (CIP2A), protein phosphatase methylesterase 1 (PME-1), and SET nuclear proto-oncogene (SET) that often are deregulated in cancers. However, how they impact cellular phosphorylation and how redundant they are in cellular regulation is poorly understood. Here, we conducted a systematic phosphoproteomics screen for phosphotargets modulated by siRNA-mediated depletion of CIP2A, PME-1, and SET (to reactivate PP2A) or the scaffolding A-subunit of PP2A (PPP2R1A) (to inhibit PP2A) in HeLa cells. We identified PP2A-modulated targets in diverse cellular pathways, including kinase signaling, cytoskeleton, RNA splicing, DNA repair, and nuclear lamina. The results indicate nonredundancy among CIP2A, PME-1, and SET in phosphotarget regulation. Notably, PP2A inhibition or reactivation affected largely distinct phosphopeptides, introducing a concept of nonoverlapping phosphatase inhibition- and activation-responsive sites (PIRS and PARS, respectively). This phenomenon is explained by the PPP2R1A inhibition impacting primarily dephosphorylated threonines, whereas PP2A reactivation results in dephosphorylation of clustered and acidophilic sites. Using comprehensive drug-sensitivity screening in PP2A-modulated cells to evaluate the functional impact of PP2A across diverse cellular pathways targeted by these drugs, we found that consistent with global phosphoproteome effects, PP2A modulations broadly affect responses to more than 200 drugs inhibiting a broad spectrum of cancer-relevant targets. These findings advance our understanding of the phosphoproteins, pharmacological responses, and cellular processes regulated by PP2A modulation and may enable the development of combination therapies.**

Reversible protein phosphorylation by kinases and phosphatases is a key mechanism in signal transduction in cancer cells. The majority of protein phosphorylation occurs at serines and threonines (Ser/Thr) (1), and the protein phosphatase 2A (PP2A)[5] is thought to be a major contributor to Ser/Thr dephosphorylation activity in human cells (2–4). PP2A is a trimeric protein complex in which a core dimer formed between the scaffolding A-subunit (PPP2R1A and PPP2R1B) and the catalytic C-subunit (PPP2CA and PPP2CB) is associated with one of the many B-subunits that facilitate the interaction of the trimer with substrate proteins (Fig. 1*A*). Besides its importance in various physiological processes, PP2A is also a critical human tumor suppressor whose inhibition promotes the malignant transformation of normal cells (2, 3, 5–8). PP2A inhibition pro-

This work was supported by The Sigrid Jusélius Foundation (to J. W. and T. A.); Ministry of Education, Culture, Sports, Science and Technology, Japan Society for the Promotion of Science KAKENHI Grants 16K08206 and 19K07017 (to S. Y. I.); Research Institute of Meijo University (to S. Y. I.); Academy of Finland Grants 292611, 310507, and 326238 (to T. A.); Academy of Finland Grant 294850 (to J. W., M. S., A. A.); the Cancer Society of Finland (to T. A. and J. W.); Natural Sciences and Engineering Research Council (NSERC) Discovery Grant RGPIN-2016-06485 (to J. R.); and Ontario Institute for Cancer Research (OICR) Biostatistics Training Initiative student fellowship (to L. R.). The authors declare that they have no conflicts of interest with the contents of this article.

This article contains Figs. S1–S7 and Tables S1–S5.

[1] Present address: Dept. of Biochemistry, University of Cambridge, Cambridge CB2 1TN, United Kingdom.

[2] Present address: Faculty of Pharmacy, Meijo University, Nagoya, Aichi 468-0073, Japan.

[3] Present address: BRIC, Biotech Research & Innovation Centre, University of Copenhagen, DK-2200 Copenhagen N, Denmark.

[4] To whom correspondence should be addressed: Turku Bioscience Centre, University of Turku, 20540 Turku, Finland. Tel.: 358-29-450-288; E-mail: jukka.westermarck@bioscience.fi.

This is an Open Access article under the CC BY license.

[5] The abbreviations used are: PP2A, protein phosphatase 2A; NPM, nucleophosmin; PIRS, phosphatase inhibition–responsive site; PARS, phosphatase activation–responsive site; PAIP, PP2A inhibitor protein; CIP2A, cancerous inhibitor of protein phosphatase 2A; PME-1, protein phosphatase methylesterase 1; GAPDH, glyceraldehyde-3-phosphate dehydrogenase; PVDF, polyvinylidene difluoride; ΔDSS, differential drug-sensitivity score; ACN, acetonitrile; FA, formic acid; AURK, aurora kinase; DSRT, drug sensitivity and resistance testing; ERK, extracellular signal-regulated kinase; PK, protein kinase; HDAC, histone deacetylase; mTOR, mechanistic target of rapamycin; BET, bromodomain and extraterminal domain.



© 2020 Kauko et al. Published under exclusive license by The American Society for Biochemistry and Molecular Biology, Inc.

motes *in vivo* tumorigenesis (9–13), and recent studies implicate PP2A as a critical determinant to kinase inhibitor responses (8, 14–16). Furthermore, orally bioavailable and nontoxic PP2A-reactivating small molecule compounds show robust antitumor effects both as monotherapies and in combination with kinase inhibitors (16–19). However, despite its critical role in cancer, and in many other diseases (20), the effects of endogenous PP2A-modulating mechanisms on phospho-signaling have not yet been systematically analyzed.

PP2A activity is affected by diverse mechanisms, including mutations (21), and interactions with endogenous proteins that modulate PP2A function. Represented in this study by CIP2A, PME-1, and SET (Fig. 1*A*), these PP2A inhibitor proteins (PAIPs hereafter) (4) have been found to suppress PP2A function toward its phosphosubstrates (3, 4, 22, 23). Despite their shared function as PAIPs, CIP2A, PME-1, and SET do not share structural features (24–26), and the mechanisms by which they inhibit PP2A activity toward their selected phosphoprotein targets are vastly different (23, 24, 26–28). Each of them may also impact PP2A activity by different mechanisms, as exemplified by PME-1 that impacts the PP2A C-subunit both by its methylesterase activity and by direct binding to the catalytic center of the PP2AC (24). However, despite their differential mode of PP2A regulation, the cancer-relevant phenotypes resulting from CIP2A, PME-1, or SET modulation can all be rescued by concomitant PP2A inhibition (5, 11, 29, 30). Furthermore, their overexpression can substitute for viral small-t as a PP2A inhibitor in human cell transformation models (10, 31, 32). Inhibition of these three PAIPs suppresses malignant cell growth and tumorigenesis *in vivo* (5, 10, 11, 30). Moreover, PP2A inhibition by CIP2A overexpression in normal mouse brains induced the symptoms and pathogenic changes resembling Alzheimer's disease (20). Based on these data, modulation of PP2A through interactions with CIP2A, PME-1, or SET has recently emerged as an attractive novel therapeutic approach for cancer and Alzheimer's disease (4, 20, 22, 23, 33, 34). However, the processes regulated by and the functional redundancy of these PP2A-modulating proteins remain poorly understood.

To address these unresolved questions, we characterized PP2A modulated phosphotargets in HeLa cells depleted of CIP2A, PME-1, and SET as well as the scaffolding A-subunit of PP2A (PPP2R1A). We identified targets in diverse cellular processes and functions, and we showed significant differences between PAIPs in their functional outcomes. To validate the global functional relevance of these modulations, we performed a drug sensitivity screen and found a broad impact on cancer cells across multiple drug target families. This resource provides insights into phosphatase-mediated signal transduction in human cells and helps advance development of rational mono- and combination therapies.

## Results

### *Identification and quantification of the PP2A-modulated targets via LC-MS/MS*

PPP2R1A is the predominant PP2A scaffold A-subunit that is required for functional PP2A complex formation (Fig. 1*A*). Unlike depletion of the catalytic PP2A subunit PPP2CA, siRNA of PPP2R1A did not cause cell lethality and, on the other hand, did not affect the PPP2CA expression (Fig. S1*A*). However, and as expected from the literature (35), PPP2R1A depletion resulted in destabilization of PPP2R5A (B56$\alpha$) and PPP2R2A (B55$\alpha$) B-subunits (Fig. S1*B*). These results confirm that PPP2R1A depletion results in comprehensive PP2A complex inhibition. To map the phosphoproteome changes regulated by the three most prevalent PAIPs, we post-transcriptionally inhibited CIP2A, PME-1, and SET (Fig. 1*A*). As confirmed by Western blot analysis, none of the targeted PAIPs interfered with each other's expression at the protein level (Fig. 1*B*) nor had notable effects on B-subunit expression (Fig. S1*B*). For MS analysis, each gene was targeted by three to four independent siRNA sequences and analyzed by MS in triplicate. Changes in peptide phosphorylation were analyzed 72 h after siRNA depletion via label-free phosphoproteomics pipeline (Fig. S1*C*) (36). The performance of the pipeline was previously validated as we observed high reproducibility between the global phosphoproteomics data and a phospho-specific antibody survey (36). We confirmed that global phosphorylation changes were largely replicated by different siRNAs targeting the same gene (Fig. S1*D*). To focus on the most reliable and robust phosphosites, we statistically selected a subset of peptides that were consistently phosphoregulated across our replicates (limma $q < 0.05$). To minimize the likelihood that the phosphoproteome was mapped in cells that were affected by transfection procedures, we selected a late time point of 72 h post-transfection for our proteomics assays. To confirm that our observations were not confounded by mitotic arrest events (37, 38), we determined mitotic index values. Importantly, more than 90% of cells in each condition remained nonmitotic at the same 72-h time point of the phosphoproteome analysis (Fig. S1*E*). Therefore, our data represent phosphoproteomes of stably PP2A-modulated interphase cells that are not cofounded by mitotic arrest. Of note, our dataset represents a single time point that does not naturally allow us to distinguish direct and indirect phosphotargets. Such single time point data are fully relevant, especially for understanding the cells in which PAIPs are differentially expressed, as is often the case between normal and cancerous tissues (4). Nevertheless, in addition to long-term siRNA treatments, we validated more immediate regulation of some of the significantly regulated phosphopeptides by pharmacological PP2A inhibition and activation. By using okadaic acid as a phosphatase inhibitor, and FTY-720 or DT-061 as PP2A activators, we were able to see consistent phosphoregulation of the selected targets as compared with siRNA data and after 12–24 h of treatment (Fig. S1, *F* and *G*).

### *Global phosphorylation changes by PP2A modulations*

In support of the global relevance in cellular Ser/Thr phosphorylation regulation, 43% of the phosphopeptides were significantly regulated by either inhibition of PAIPs or PPP2R1A ($q < 0.05$), and 57% of the phosphoproteins had at least one differentially-regulated phosphopeptide. The catalogue of differentially-regulated phosphopeptides ($q < 0.05$) is included as Table S1. Depletion of the PPP2R1A resulted in a robust increase in the average phosphorylation level across the HeLa cell phosphoproteome (Fig. 1*C* and Fig. S1, *D* and *H*). In con-

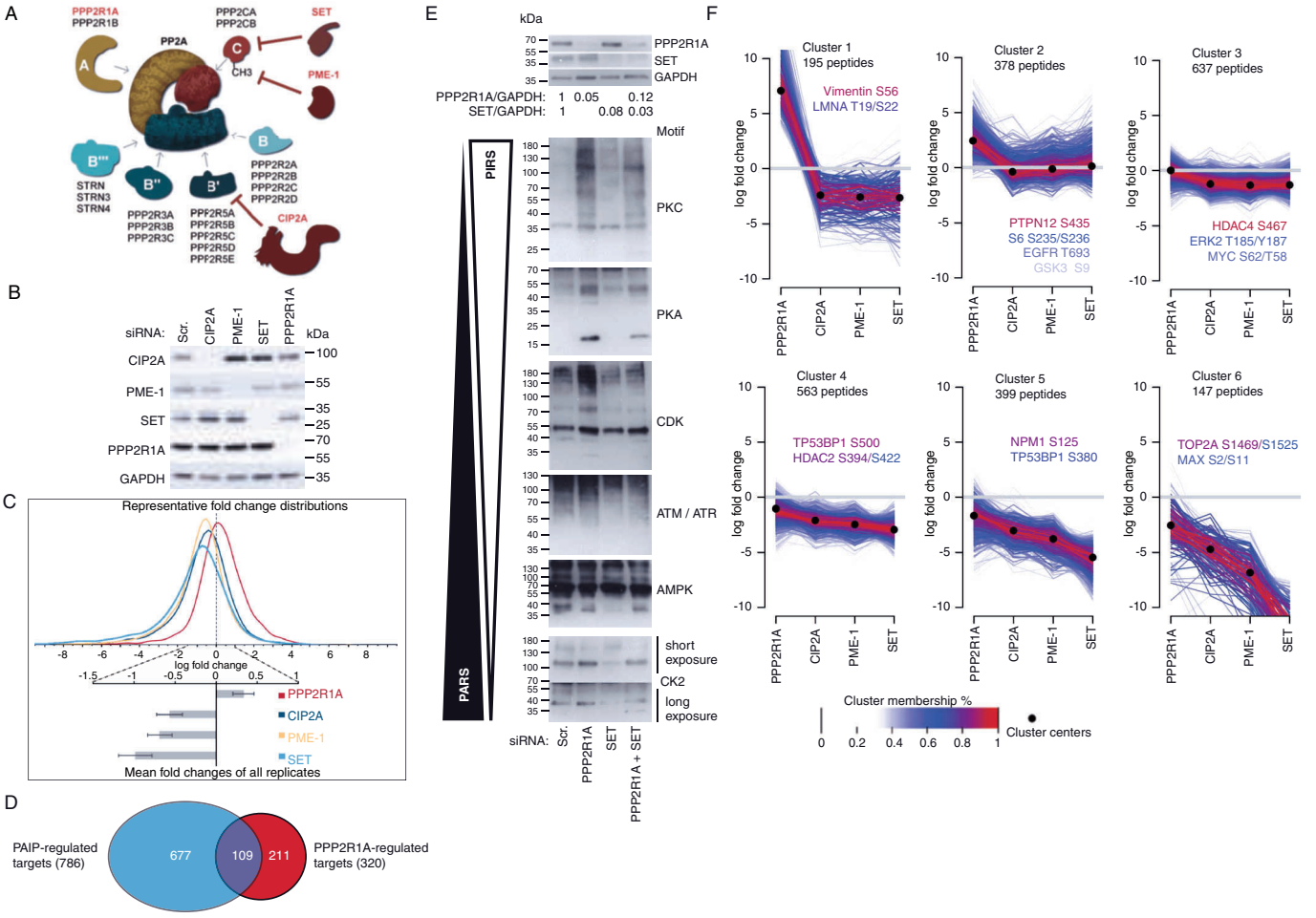


**Figure 1. PPP2R1A or PAIP inhibition regulates largely nonoverlapping phosphosites.** *A*, schematic presentation of PP2A complex and its activity regulation by subunit composition and by endogenous inhibitor proteins (*PAIPs*). Whereas B-subunits regulate substrate specificity of the trimeric PP2A complex, each PAIP (CIP2A, PME-1, and SET) regulates PP2A complex activity by a distinct mechanism. *B*, Western blot analysis of selectivity of siRNAs for the studied PP2A proteins in HeLa cells 72 h after siRNA transfection. *C*, PPPP2R1A or PAIP inhibition causes global shift in HeLa cell phosphoproteome. Shown are fold change distributions of representative replicates (*top*) and mean log 2-fold changes of all replicates (*bottom*). Fig. S1*H* shows fractions of differentially regulated phosphosites for each condition. *D*, Venn diagram shows the overlap between PPP2R1A and PAIP-regulated peptides at $q < 0.05$. Total number of significantly-regulated peptides are shown in *parentheses*. *E*, analysis of targets of different kinases by phosphomotif antibodies arranged from the most PPP2R1A-responsive phosphoproteins (PIRS) to the most SET-responsive phosphoproteins (PARS) in descending order. *F*, unsupervised soft clustering analysis of the high-confidence phosphoproteome data into six clusters. Cluster membership percentage is indicated by a *color scale*, and representative peptides are listed *inside the plots*. Cluster centers (indicated by *black dots*) exhibit mainly either up-regulation (*cluster 2*) or down-regulation (*clusters 3–6*). *Cluster 1* instead shows the pattern of phosphoregulation for peptides that respond to both PP2A inhibition and activation. Cluster membership of each clustered phosphopeptide is shown in Table S1.

trast to PPP2R1A, cells that were depleted of any of the PAIPs displayed global dephosphorylation (Fig. 1*C* and Fig. S1, *D* and *H*). These results indicate that the dominant function of PAIPs is indeed the inhibition of dephosphorylation activity, thus validating the previous findings that the functional effects of these proteins can be rescued by concomitant PP2A inhibition (5, 11, 29, 30) and that they can substitute for small-t as a PP2A inhibitor (10, 31, 32).

Among PAIPs, SET was the most robust inhibitor of protein dephosphorylation that regulated 30.5% of the phosphopeptides (Fig. S1*H*). In accord with a common regulatory mechanism with SET (*i.e.* PP2A inhibition), the majority of the CIP2A and PME-1 target peptides overlapped with the target peptides of SET (Fig. S1*I*). Nevertheless, CIP2A regulated 70 unique targets not significantly regulated by PME-1, and PME-1 regulated 115 targets that were not regulated by CIP2A (Fig. S1*I*). These nonredundant targets could be apparent due to the differential selectivity of CIP2A and PME-1 for different PP2A trimer complexes (23, 24, 26–28). The larger number of SET targets compared with CIP2A and PME-1 (Fig. S1*I*) may be at least partly due to the direct inhibition of the catalytic activity of PP2Ac by SET (27, 28) and the limited selectivity toward specific B-subunit–containing PP2A trimers, as is the case with PME-1 or CIP2A (10, 26, 39). Importantly, as only few phosphopeptides that were consistently and significantly regulated by PAIPs exhibited increased phosphorylation (0.5–2.7%) (Fig. S1*H*), these data indicate that PAIP inhibition cannot be compensated by increased kinase activity toward another set of phosphotargets, at least at the 72-h time point.

### *PP2A inhibition- and activation-responsive phosphotargets*

Accumulating data show that specific phosphorylation sites tend to be predominantly phosphorylated, or dephosphorylated, depending on the amino acid context of the phosphorylated

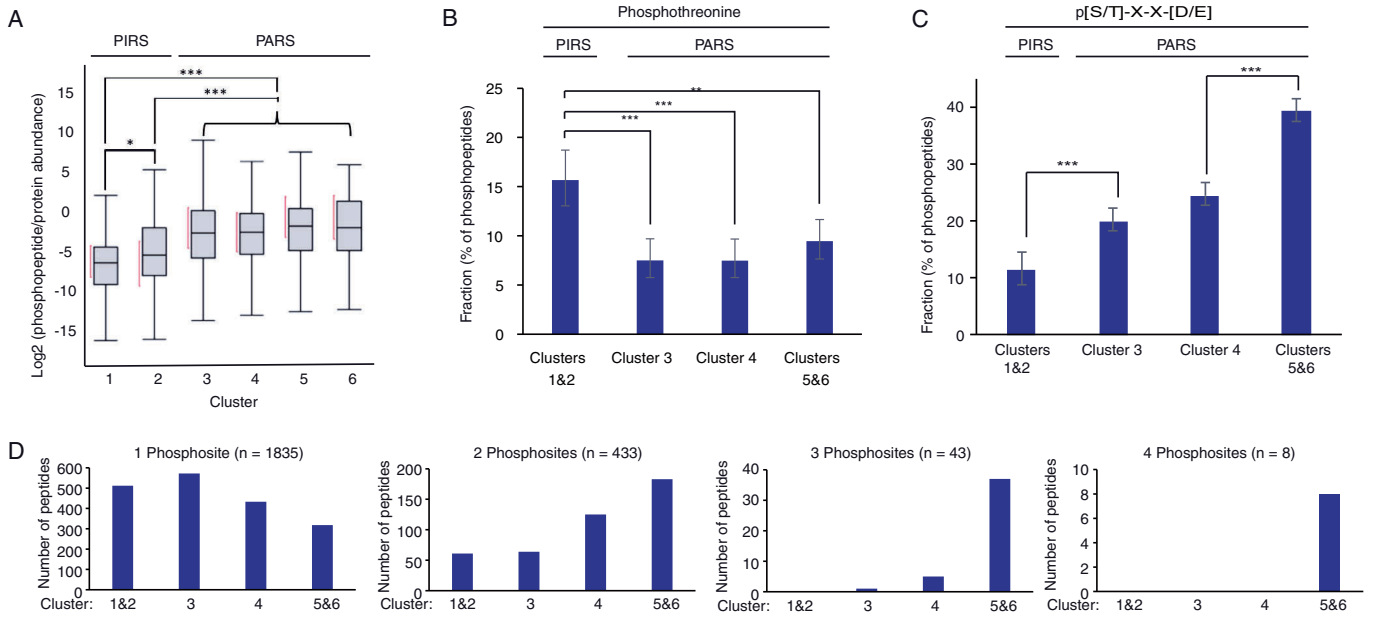


**Figure 2. Sequence context analysis of the phosphorylation sites differentially regulated by PPP2R1A or by PAIPs.** *A–C*: PIRS, phosphatase inhibition responsive site; PARS, phosphatase activation responsive site. *A,* phosphopeptide abundances in control samples (no PP2A modulations) divided by corresponding protein abundances (quantified by ≥2 peptides in the sample without phosphopeptide enrichment) for each cluster. This information was available for 140, 179, 314, 292, 206, and 78 peptides for clusters 1–6, respectively. *, $p < 0.05$, and ***, $p < 0.001$, in Tukey-Kramer test for pairwise comparisons of mean values between clusters. *B,* analysis of the fraction of phosphothreonines of all phosphorylation sites in each cluster reveals significant enrichment in PIRS clusters having lower baseline phosphorylation based on *A*. *Error bars* represent 95% confidence intervals. **, $p < 0.01$, and ***, $p < 0.001$ in $\chi^2$ test. *C,* analysis of fraction of phosphosites with acidophilic p(S/T)*XX*(D/E) motif in each cluster shows association with PARS clusters. *D,* number of peptides with 1–4 phosphosites associated with each cluster.

site (40–44). Furthermore, previous global phosphoproteome analyses demonstrated that a majority of phosphosites had either high or low stoichiometry, although intermediate stoichiometry was rare (1, 42). Therefore, we hypothesized that PP2A inhibition would primarily affect those sites that are not constitutively occupied by a phosphate (phosphatase inhibition–responsive site (PIRS)), whereas inhibition of PAIPs might preferentially regulate high-stoichiometry phosphosites (phosphatase activation–responsive site (PARS)).

In support of this hypothesis, the majority of the same peptides that were regulated by PPP2R1A inhibition were not regulated by depletion of PAIPs and vice versa (211/320 PPP2R1A targets (66%) and 568/677 PAIP targets (84%)) (Fig. 1*D*). These findings were methodologically and independently validated by phospho-motif antibodies showing that PPP2R1A depletion increased the phosphorylation of a different set of phosphomotifs compared with those that were dephosphorylated by increased PP2A activity in SET-depleted cells (Fig. 1*E*).

To analyze the characteristics of PIRS and PARS phosphosites, we performed an unsupervised soft clustering analysis (45). Consistent with the observation of distinct targets of PPP2R1A and PAIPs (Fig. 1*D*), the peptides in five of the six unsupervised clusters were regulated exclusively toward either increased phosphorylation (by PPP2R1A inhibition in cluster 2) or dephosphorylation (by inhibition of PAIPs in clusters 3–6) (Fig. 1*F*). As an exception, the peptides in cluster 1, consisting of 8.5% of all clustered phosphopeptides, followed the pattern of being responsive to both PP2A inhibition and activation (Fig. 1*F*). Furthermore, we observed that the target peptides in clusters 5 and 6 were most potently impacted by SET, followed by PME-1, and then CIP2A (Fig. 1*F*), supporting the partially differential outcomes via inhibition of each PAIP (Fig. S1, *H* and *I*). Notably, the clustering analysis remained robust when normalizing the phosphopeptides in each cluster relative to total protein abundance of the nonenriched sample for proteins in which we could identify ≥2 unenriched peptides (Fig. S2). Thus, the phosphosite clustering represents true phosphorylation stoichiometry changes rather than global changes in protein abundance. Finally, to ensure that these findings were not limited to the current model of HeLa cells, we performed soft clustering of PP2A-modulated phosphoproteome from A549 lung cancer cell line from a previous study (16). Similar to HeLa cells, the clusters were characterized by either up-regulation or down-regulation but not both in the same cluster. Consistently, most prominent up-regulations were observed in PPP2R1A-depleted cells and down-regulations were observed in PAIP-depleted cells (Fig. S3).

### *Phosphorylation stoichiometry and amino acid context of PIRS and PARS phosphopeptides*

Next, we further assessed phosphorylation stoichiometry and amino acid context of PP2A-modulated phosphopeptides in each cluster. To determine baseline phosphorylation stoichiometry, we assessed cells with no modulation of PP2A activity (*i.e.* cells transfected with scrambled siRNAs). Supportive of our conclusions, peptides belonging to clusters 1 and 2 (Fig. 1*F*) had a significantly lower baseline phosphopeptide/total protein abundance than peptides in clusters 3–6 (Fig. 2*A*). The broad classification of most of the PP2A-modulated peptides as PIRS or PARS (except for those in cluster 1) was also supported by analysis of peptide sequences for determinants known to impact phosphate occupancy (40–44). Previous studies indi-

cate that a higher PP2A/kinase activity ratio is associated with threonines rather than serines (40, 43, 44), whereas acidophilic kinase target sites exhibit a higher phosphate occupancy on average (42). To analyze our data according to these parameters, clusters 1 and 2 (cluster 1 & 2 hereafter) and clusters 5 and 6 (cluster 5 & 6 hereafter) were combined to yield four nearly equally-sized clusters together with clusters 3 and 4. Using these four clusters, we found that peptides from cluster 1 & 2, having lower phosphorylation stoichiometry (PIRS) (Fig. 2*A*), were indeed enriched in phosphothreonines (Fig. 2*B*), and somewhat on basophilic kinase targets (Fig. S4). However, acidophilic kinase targets were enriched in PARS peptides (Fig. 2*C* and Fig. S4) that had higher phosphate stoichiometry in unperturbed conditions (Fig. 2*A*). Finally, we observed that peptides having three or four phosphates were enriched among PARS clusters, whereas peptides with only one phosphosite were associated with PIRS clusters, and with cluster 3 exhibiting less prominent PAIP effects.

Collectively, these results (Figs. 1 and 2) are consistent with the previously identified determinants of phosphorylation stoichiometry (1, 40–44). In the context of PP2A-mediated phosphoregulation, these data show that a significant fraction of serine/threonine phosphosites are primarily sensitive either to PP2A inhibition or activation, but not to both. Furthermore, we reveal that phosphosite amino acid sequence can be predictive of substrates regulated by different PAIPs. As an example, the SET-dominated cluster 5 & 6 (Fig. 1*F*) were most strongly enriched for acidophilic kinase targets (Fig. 2*C* and Fig. S4) and for peptides with several clustered phosphosites (Fig. 2*D*).

### *PP2A-mediated control of cellular processes*

To investigate the biological processes that are affected in cells with long-term PP2A modulation, we analyzed the enrichment of pathways and biological processes using the g:Profiler software (46). PP2A-modulated targets were found in a large number of cellular processes and functions, including regulation of translation, RNA metabolism, DNA repair, transcription, heat response, apoptosis, and host–virus interactions (Fig. 3*A*). Interestingly, most of phosphopeptides from the similarly-behaving cluster (Fig. 1*F*) are associated with the same cellular processes, indicating that proteins involved in the same biological process respond similarly to PP2A modulations (Fig. 3*A*). To exclude the possibility of technical variation affecting the clustering analysis, we examined whether selective association of cellular processes with either PP2A or PAIP inhibition was also observed by using significantly-regulated individual peptides. Consistent with the analysis with clustered phosphopeptides, most of the cellular processes were associated selectively either by PPP2R1A or PAIP inhibition, but not by both (Fig. S5). The data also identified processes selectively regulated by SET, PME-1, and CIP2A (Fig. 3*B* and Fig. S5), providing clear indications for nonredundant cellular functions for PAIPs.

Interestingly, in contrast to most other cellular functions that responded primarily to either PPP2R1A or PAIP inhibition (Fig. 3*A* and Fig. S5), mRNA processing (including *e.g. Regulation of RNA stability* and *RNA processing and splicing*) was associated with both inhibition and activation of PP2A (Fig. 3*A* and Fig. S5). Nevertheless, when assessed at the level of individual proteins, PP2A inhibition almost exclusively increased phosphorylation of cancer-related splicing factors (*e.g.* HNRNPA1, SRSF3, and RBM4) (47), whereas a distinct set of splicing factors was found to be dephosphorylated upon depletion of the PAIPs (Fig. 4*A*). RBM25 was the only target in which the same peptide (Ser-677/Ser-683) was subject to regulation by both PPP2R1A and PAIPs. Therefore, the division of PP2A-modulated target proteins to either as PIRS or PARS, holds true also for splicing factors, albeit as a process RNA splicing is most likely responsive to both PP2A inhibition and activation through these nonoverlapping targets.

As RNA-binding proteins were profoundly represented in PP2A-modulated targets, and RNA processing has an important role in cancer (48), we looked for an example where PP2A-mediated phosphorylation changes might impact the cancer-relevant function of an RNA-binding protein. Nucleophosmin (NPM) is a nucleolar RNA-binding protein implicated in cancer (49). In our data, serines 254 and 260 in the C-terminal domain of NPM were significantly regulated by PP2A inhibition (Fig. 4*B*). Intriguingly, upon transient transfection WT and double-alanine mutants of NPM–GFP displayed the prototypical nucleolar localization pattern in MDA–MB-231 cells; phosphomimic aspartate mutations of these PP2A-regulated sites induced similar translocation of NPM to nucleoplasm as is seen with the oncogenic mutations of the NPM C-terminal domain (Fig. 4, *B* and *C*) (49). As a control, all exogenous NPM proteins were tested to be expressed at comparable protein levels (Fig. S6*A*). Thus, in cancer cells with inhibited PP2A, but are genetically WT for NPM, PP2A inhibition–induced hyperphosphorylation of NPM could result in similar oncogenic consequences as with NPM C-terminal mutations (49).

Enrichment of canonical signaling pathways and kinase targets between different clusters was additionally evaluated by Ingenuity Pathway Analysis software and the NetworKIN kinase target prediction tool (50). The target proteins in each pathway predicted to be regulated based on NetworKIN are listed in Table S2. Interestingly, the PIRS and PARS clusters associated with distinct canonical signaling pathways. Among the kinase signaling pathways, PTEN signaling, AKT targets, and PKC targets were most clearly associated with PIRS clusters, whereas ERK signaling associated predominantly with PARS cluster 3 (Fig. 4, *D* and *E*). ERK pathway inhibition by PAIP inhibition is consistent with recent cancer data using either PME-1 siRNA (51) or PP2A-reactivating compounds (17). In contrast to PIRS clusters enriched in most kinase-signaling pathways, PARS clusters were associated with processes related to DNA repair. Canonical DNA repair-associated pathways and DNA-PK targets were enriched in clusters 4–6 (Fig. 4, *D* and *E*). DNA-PK was also among the most enriched kinases predicted to phosphorylate peptides with multiple phosphorylation sites (Fig. S6*B*). The analysis indicates that DNA damage–response proteins are dephosphorylated upon PAIP depletion; however, their phosphorylation cannot be increased from basal line levels by PPP2R1A inhibition. This finding is consistent with recent studies characterizing DNA damage response as a cellular process regulated by dephosphorylation of constitutively-phosphorylated sites (52). Furthermore, a

A

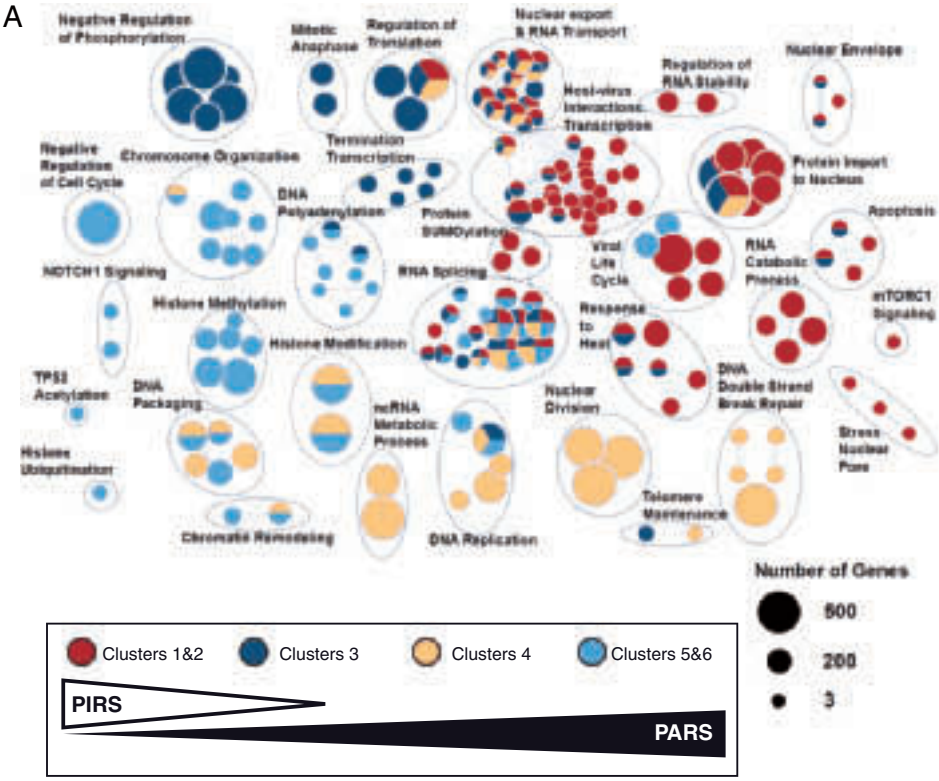


B

| CIP2A | Biological Process (GO) | | |
|---|---|---|---|
| *GO-term* | *description* | *count in gene set* | *false discovery rate* |
| GO:0007010 | cytoskeleton organization | 25 of 953 | 1.69e-08 |
| GO:0006996 | organelle organization | 44 of 3131 | 1.90e-08 |
| GO:0097435 | supramolecular fiber organization | 14 of 383 | 7.26e-06 |
| GO:0071840 | cellular component organization or biogenesis | 53 of 5342 | 1.18e-05 |
| GO:0031032 | actomyosin structure organization | 8 of 97 | 2.23e-05 |

| PME-1 | Biological Process (GO) | | |
|---|---|---|---|
| *GO-term* | *description* | *count in gene set* | *false discovery rate* |
| GO:0090304 | nucleic acid metabolic process | 64 of 3941 | 1.56e-10 |
| GO:0006996 | organelle organization | 56 of 3131 | 1.70e-10 |
| GO:2000112 | regulation of cellular macromolecule biosynthetic process | 62 of 4050 | 2.62e-09 |
| GO:0045934 | negative regulation of nucleobase-containing compound m... | 35 of 1424 | 4.09e-09 |
| GO:0009889 | regulation of biosynthetic process | 63 of 4337 | 7.96e-09 |

| SET | Biological Process (GO) | | |
|---|---|---|---|
| *GO-term* | *description* | *count in gene set* | *false discovery rate* |
| GO:0090304 | nucleic acid metabolic process | 217 of 3941 | 2.01e-39 |
| GO:0006139 | nucleobase-containing compound metabolic process | 223 of 4551 | 2.74e-33 |
| GO:0046483 | heterocycle metabolic process | 224 of 4716 | 1.35e-31 |
| GO:0006725 | cellular aromatic compound metabolic process | 224 of 4754 | 3.47e-31 |
| GO:0034641 | cellular nitrogen compound metabolic process | 233 of 5126 | 8.54e-31 |

**Figure 3. Regulation of cellular processes and pathways.** *A,* cellular processes and pathways enriched in proteins phosphoregulated by PP2A modulations. The majority of enriched cellular functions was associated predominantly with only one cluster, indicating that biological functions can also be roughly divided to be responsive to either PP2A inhibition or activation. *B,* five most significantly-enriched biological process GO terms based on phosphoproteomes significantly ($q$ <0.05) regulated by CIP2A, PME-1, or SET.

recent study demonstrated that PP2A activity counteracts DNA damage response in yeast (53).

Collectively, PP2A modulations were found to impact the proteome in diverse cellular pathways and processes. Consistent with differential regulation of individual target peptides, different cellular functions and pathways can also be divided based on whether they primarily respond to PPP2R1A or PAIP inhibition (see summary scheme in Fig. 7).

### *Cytoplasm–nuclear gradient of PP2A modulation*

Pathway analysis of PP2A-modulated targets revealed an interesting observation that cytoplasmic kinase signaling associated with PIRS clusters, whereas nuclear processes seemed to associate with PARS clusters (Figs. 3*A* and 4, *D* and *E*). PPP2R1A localizes to both the cytoplasm and nucleus; CIP2A is predominantly cytoplasmic, and both SET and PME-1 are nuclear (Fig. 5*A*). Thus, we postulated that differential regulation of cytoplasmic and nuclear phosphoproteome targets could be at least partly linked to differential localization of PAIPs. To examine this uncharacterized aspect of PP2A biology, we assessed the subcellular protein localization of the phosphoproteome target proteins in different clusters. Whereas the targets of the PIRS cluster appeared to be indeed

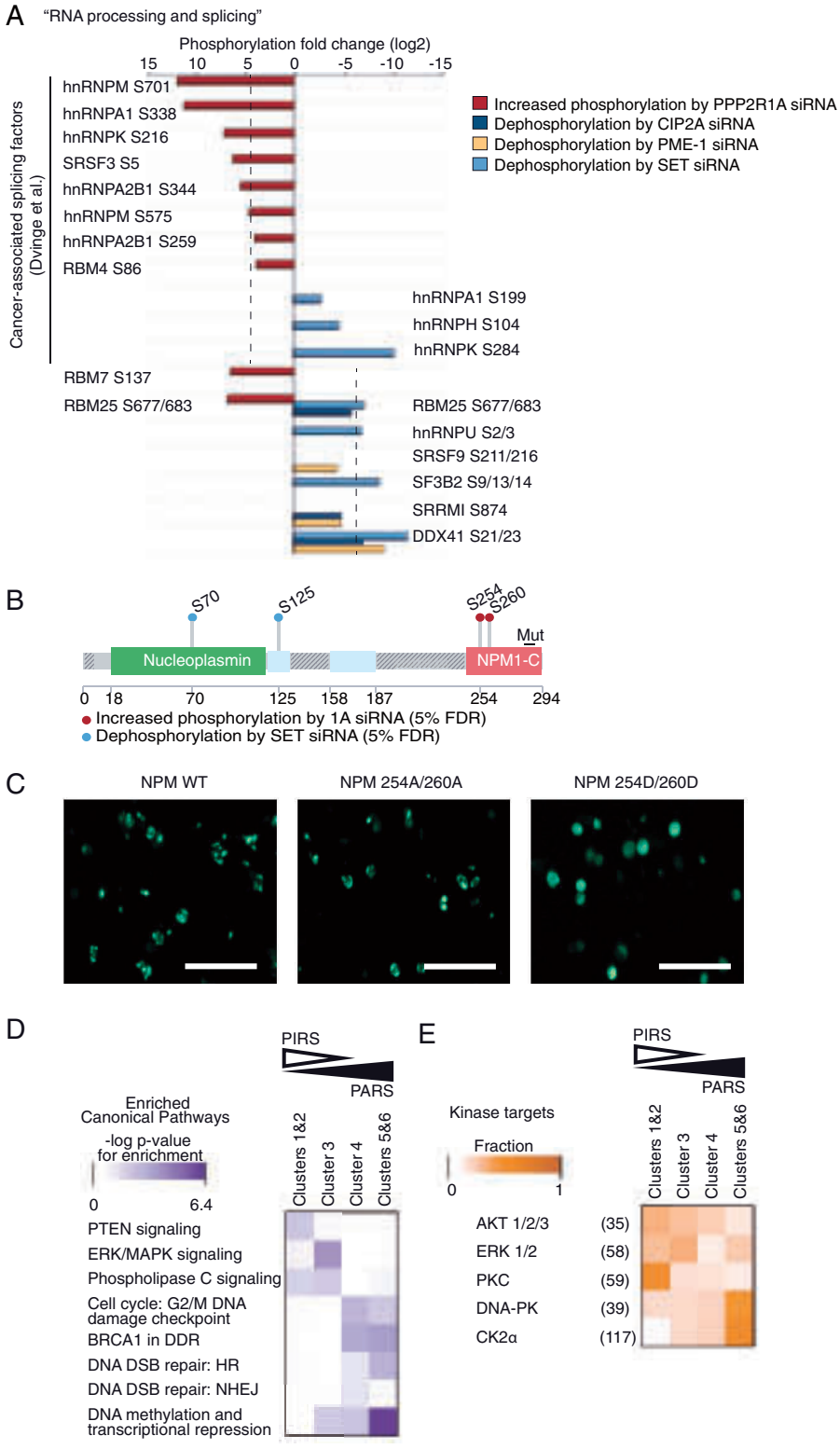


**Figure 4. PP2A regulates RNA-processing factors and canonical pathways.** *A,* differentially-regulated phosphosites ($q < 0.05$) on proteins in the enriched category "*RNA processing and splicing*" from g:Profiler analysis. At the level of significantly-regulated peptides, PPP2R1A and PAIPs regulate different splicing factors. *B,* schematic presentation of SET- and PPP2R1A-regulated phosphosites on NPM. *Mut,* region most commonly mutated in NPM resulting in nucleoplasmic localization of the protein. *C,* analysis of nuclear distribution of WT and indicated NPM mutants in transiently-transfected MDA–MB-231 cells. Phosphorylation mimicking D mutants display similar nucleoplasmic localization than known cancer mutants of NPM. *Scale bar,* 20 μm. *D* and *E*, differential association of selected canonical pathways (*D*), and kinase targets (*E*) with either PIRS or PARS clusters.

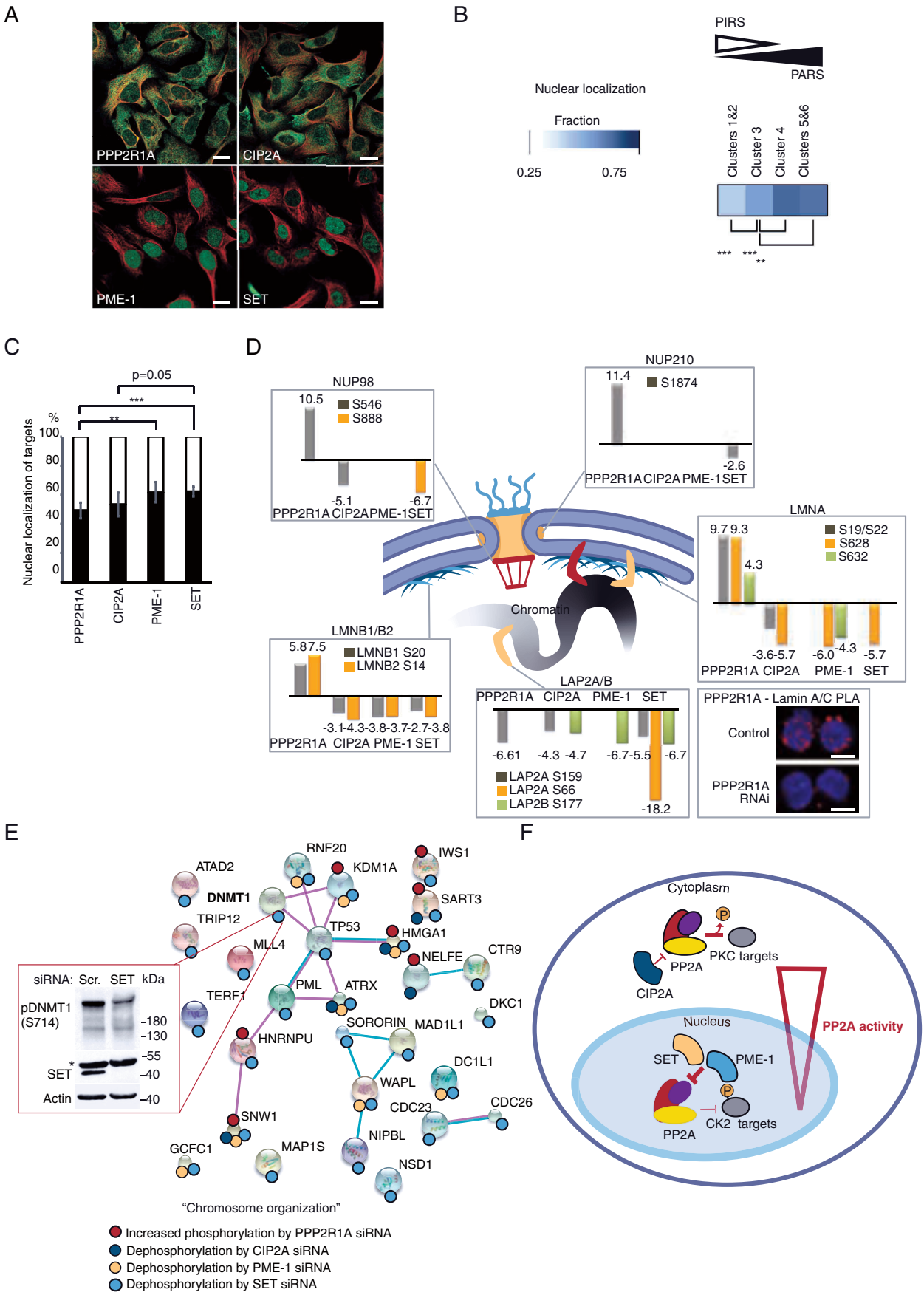
A
PPP2R1A
CIP2A
PME-1
SET
B
PIRS
PARS
Nuclear localization
Fraction
0.25
0.75
Clusters 1&2
Cluster 3
Cluster 4
Clusters 5&6
*** *** **
C
p=0.05
***
**
%
Nuclear localization of targets
100
80
60
40
20
0
PPP2R1A
CIP2A
PME-1
SET
D
NUP98
10.5
S546
S888
-5.1
-6.7
PPP2R1A CIP2A PME-1 SET
NUP210
11.4
S1874
-2.6
PPP2R1A CIP2A PME-1 SET
LMNA
9.7 9.3
4.3
S19/S22
S628
S632
-3.6 -5.7
-6.0 -4.3
-5.7
PPP2R1A CIP2A PME-1 SET
Chromatin
LMNB1/B2
5.87.5
LMNB1 S20
LMNB2 S14
-3.1 -4.3 -3.8 -3.7 -2.7 -3.8
PPP2R1A CIP2A PME-1 SET
LAP2A/B
PPP2R1A CIP2A PME-1 SET
-6.61 -4.3 -4.7
-6.7 -5.5
-6.7
-18.2
LAP2A S159
LAP2A S66
LAP2B S177
PPP2R1A - Lamin A/C PLA
Control
PPP2R1A RNAi
E
ATAD2
RNF20
KDM1A
IWS1
SART3
DNMT1
TRIP12
TP53
HMGA1
MLL4
NELFE
CTR9
PML
ATRX
TERF1
DKC1
SORORIN
MAD1L1
HNRNPU
DC1L1
WAPL
CDC23
CDC26
SNW1
NIPBL
GCFC1
MAP1S
NSD1
siRNA: Scr. SET kDa
pDNMT1 (S714)
-180
-130
SET
-55
-40
Actin
-40
"Chromosome organization"
Increased phosphorylation by PPP2R1A siRNA
Dephosphorylation by CIP2A siRNA
Dephosphorylation by PME-1 siRNA
Dephosphorylation by SET siRNA
F
Cytoplasm
P
PKC targets
PP2A
CIP2A
Nucleus
PP2A activity
SET
PME-1
P
CK2 targets
PP2A

dominantly cytoplasmic, the PARS clusters were highly enriched in nuclear proteins (Fig. 5*B*). Nuclear PME-1 and SET had the most prominent effects on clusters 4–6 (Fig. 1*F*), and these clusters were particularly enriched for nuclear proteins (Fig. 5*B*). In contrast, the predominantly cytoplasmic CIP2A had a less potent effect in clusters 4–6. The correlation between the nuclear localization of PME-1 or SET and their nuclear target proteins was also apparent at the level of the differentially-regulated peptides (Fig. 5*C*).

To assess how differential subcellular distribution of processes associated with PIRS and PARS clusters shows up at the individual target proteins, we visualized PP2A-modulated targets in either the cytoplasm–nuclear border or in nuclear protein complexes. As indicated previously by g:Profiler analysis of cellular processes (Fig. 3*A* and Fig. S5), nuclear lamina organization was one of the rare processes that responded to both PP2A and PAIP inhibition indicating for nearly equal kinase and phosphatase activities at the nuclear– cytoplasmic interphase. Previously, PAIPs CIP2A (54) and PME-1 (55) were shown to interact with one of the main constituents of nuclear lamina LMNA, and here we further validated the physical proximity of PPP2R1A with LMNA on the nuclear envelope using proximity ligation assay (Fig. 5*D*, *inset*). Phosphorylation of LMNA at phosphosites Ser-22, Ser-628, and Ser-632 was indeed significantly affected by both PP2A inhibition and activation (Fig. 5*D*). In addition, we identified regulation of LMNA Ser-3 and Ser-652 only by PPP2R1A and of Ser-390 and Ser-392 only by SET (Table S1). In addition to LMNA, LMNB1 and LMNB2, also the nuclear pore proteins NUP98 and NUP210 were regulated by both PP2A activation and inhibition at the same phosphosite (Fig. 5*D*). Additionally, the inhibition of PAIPs resulted in dephosphorylation of the nuclear lamina anchor proteins LAP2A and LAP2B (Fig. 5*D*). To validate the MS data, LMNA phosphorylation was shown by Western blotting to be inhibited by either PME-1 siRNA or CRISPR/Cas9 targeting (Fig. S6, *C* and *D*).

As an example of nuclear PARS processes, we focused on "chromosome organization," which in g:Profiler analysis was strongly enriched in the SET target proteins (Fig. S5). As a remarkable example, in the p53-associated protein complex, phosphorylation of every individual protein was regulated by SET (Fig. 5*E*). We validated SET-mediated inhibition of dephosphorylation of one target, Ser-714 of DNMT1, using a phospho-specific antibody in A549 lung cancer cells (Fig. 5*E*, *inset*). About 50% of the proteins associated with chromosome organization were also regulated by the nuclear PME-1 and were consistent with the gradient model; both CIP2A and PPP2R1A had fewer targets in these processes (Fig. 5*E*).

In summary, these data reveal a cytoplasm–nuclear gradient of PP2A activity. Based on data, the highly-phosphorylated peptides in clusters 4–6 (Fig. 2*A*), which are enriched both on nuclear proteins (Fig. 5*B*) and CK2 targets (Fig. 4*E*), are most responsive to SET and PME-1 inhibition (Fig. 5*C*). Cytoplasmic peptides instead were more frequently found to be regulated by CIP2A (Fig. 5*C*) and to be associated with low phosphate occupancy (Fig. 2*A*), and PKC target sequences (Fig. 4*E*). These data are consistent with previously shown localization of CK2 and PKC (56, 57). Also consistent with the gradient model, nuclear envelope target peptides, between the cytoplasm and nucleus, were found to be subject to phosphoregulation by both PP2A inhibition and activation.

### *Drug responses as surrogate measure for functional impact of PP2A across diverse cellular pathways*

Results above reveal a role for PP2A modulations in a wide range of cellular processes and pathways, many of them involved in cancer cell drug responses. This indicates that PP2A modulations might result in more efficient drug responses. As a systematic approach to assess how globally PP2A affects cellular pathways and processes, we used impact of PP2A modulations on cellular responses to 306 individual drugs as a surrogate functional readout. For this purpose, we used the drug sensitivity and resistance testing (DSRT) platform (58) in which combined effects of drugs and PP2A modulations on cell viability were measured by the CellTiter-Glo assay. By using the same platform, we recently demonstrated a link between PP2A activity and drug responses in KRAS-mutant lung cancer cell across 200 kinase inhibitors (16). The RNAi treatments were identical to those applied for phosphoproteome profiling, and the differential drug-sensitivity score (ΔDSS) (59) was calculated between the treated and control samples. We excluded 68/306 tested drugs that elicited no significant effect on cell viability, regardless of the PP2A modulation (Table S3). The shift in the dephosphorylation balance (Fig. S1*H*) was used as an indicator of dephosphorylation activity, and the drugs were ranked by uncentered Pearson's correlation between the dephosphorylation activity and the changes in ΔDSS profile (Fig. 6*A*). The drugs that exhibited synergy with PAIP depletion appeared at the top of the "correlation rank" (Fig. 6*A*, *red*), whereas the drugs at the bottom exhibited synergy with PPP2R1A inhibition (*blue*). Enrichment scores were calculated for selected drug

**Figure 5. Differential spatial distribution of PP2A-modulated targets.** *A,* subcellular localizations of PPP2R1A and PAIPs, retrieved from RRID:SCR_006710. *PPP2R1A*: CAB018599: U-2 OS, image 2; *CIP2A*: HPA039570: U-2 OS, image 1; *PME-1*: CAB004541: U-2 OS, image 1; *SET*: HPA063683: U-2 OS, image 1. *Scale bar,* 10 $\mu$m. *B,* analysis of nuclear proteins in each cluster demonstrates association between PARS and nuclear localization of the target protein (*clusters 4–6*). Based on lower frequency of nuclear proteins in cluster 1 & 2, it is apparent that cytoplasmic proteins are under higher dephosphorylation activity than nuclear proteins. *C,* fraction of nuclear proteins in the proteins with differentially-regulated phosphopeptides for each condition. *A* and *C*, **, $p < 0.01$, and ***, $p < 0.001$, in $\chi^2$ test. *D,* differentially-regulated phosphosites on proteins in the enriched category *Nuclear envelope organization*. Proximity ligation assay of PPP2R1A and Lamin A/C protein association at nuclear lamina is shown in the *inset*; with PPP2R1A siRNA as a PLA staining specificity control. *Red dot* indicates close proximity of PPP2R1A and Lamin A/C proteins. *Scale bar*, 10 $\mu$m. *E, Chromosome organization* indicates an example of chromatin-associated protein complexes regulated dominantly by nuclear PP2A inhibitors SET and PME-1. *Inset* shows Western blot analysis of DNMT1 Ser-714 phosphorylation from A549 cells transfected with SET siRNA for 72 h. * denotes unspecific band. *F,* schematic presentation of the observed differential cytoplasm–nuclear association of phosphorylation patterns of PP2A targets. Based on data, highly-phosphorylated peptides in clusters 4–6 that are most responsive to SET and PME-1 inhibition are enriched in nucleus. Highly-phosphorylated peptides associated with cluster 5 & 6 were enriched on CK2 targets. Cytoplasmic peptides instead were more frequently found to be regulated by CIP2A and to be associated with low phosphate occupancy and PKC target sequences. Together, these results indicate for a gradient where cytoplasmic PP2A is more weakly inhibited (*e.g.* by CIP2A) than nuclear PP2A (*e.g.* by SET and PME-1).

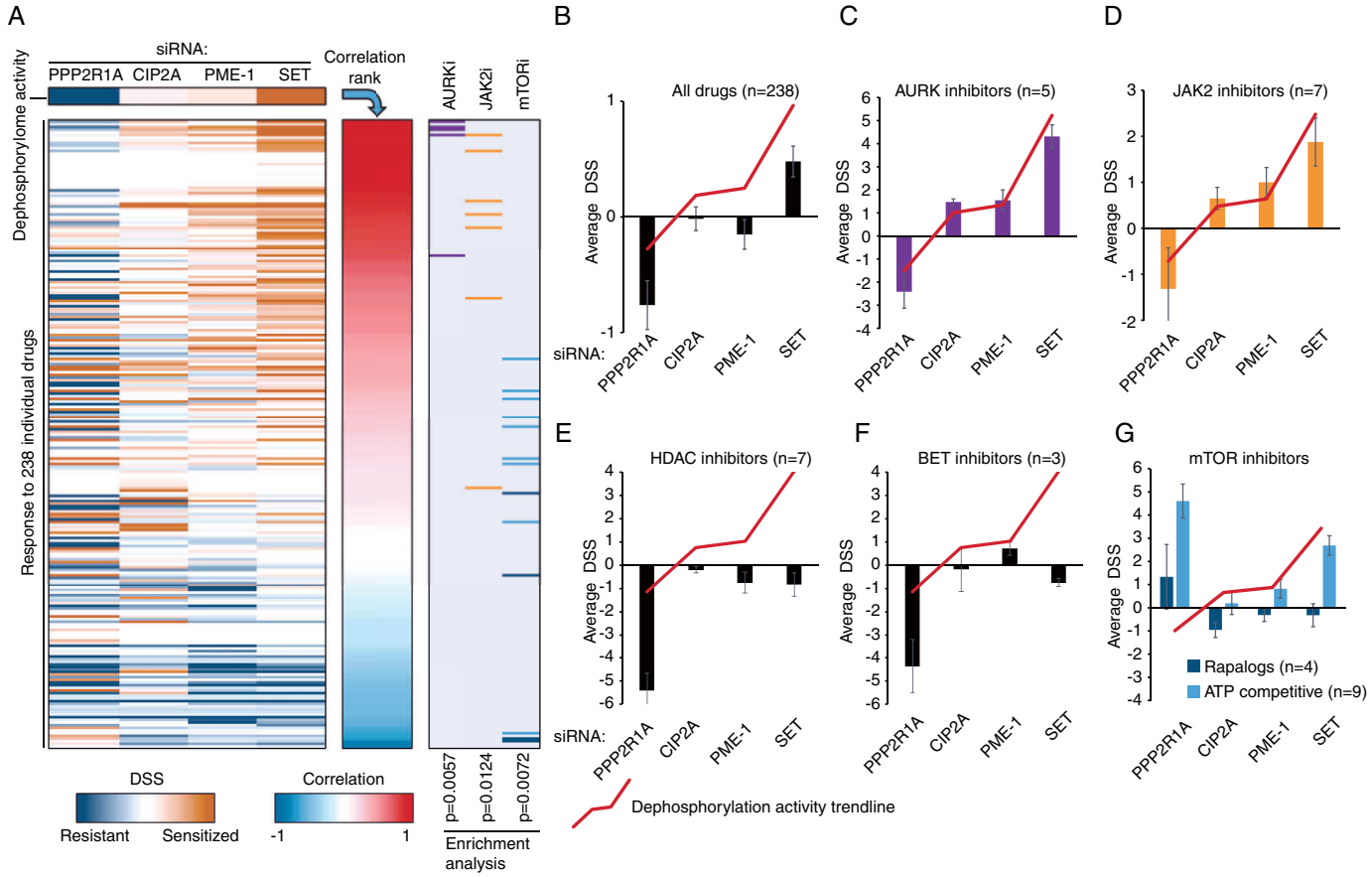


**Figure 6. Effects of PPP2R1A and PAIPs in global drug responses.** *A,* drug-sensitivity scores (Δ*DSS*) of 238 cancer drugs in HeLa cells are ranked by correlation to the dephosphorylation activity index derived from differentially-regulated peptides for each gene, which is represented as *the top color bar* in *A* and as a *red line* in *B–G*. Correlation rank demonstrates that drugs can be ranked according to the dependence of their response on the type of PP2A modulation. Significant enrichment of selected drug groups based on their dependence is shown in the *right panel*. *B,* average ΔDSS over all 238 drugs demonstrating that on average drugs follow the dephosphorylation activity (from S1H) in their efficacy. *C–G*, selected drug responses for indicated drugs in PP2A-modulated HeLa cells. Shown is mean ± S.D. of response to different drugs targeting the indicated mechanism. The cellular sensitivity for Aurora kinase (*AURK*) inhibitors (*C*) and JAK2 inhibitors (*D*) followed closely the dephosphorylation activity by the same PP2A modulations. HDAC (*E*) and BET (*F*) inhibitors constitute prototypic examples of drug classes for which PPP2R1A inhibition drove resistance, whereas the PAIP inhibition did not result in drug sensitization. *G,* ATP-competitive mTOR inhibitors show paradoxical dependence where both PPP2R1A and SET inhibition sensitize to drug action. Rapalogs show differential dependence from ATP competitive inhibitors.

groups in the ranked list (Fig. 6*A*, *right panel*). All individual drug responses are listed in Table S3.

Notably, PP2A modulations impacted cellular viability responses to drugs targeting a wide range of cellular pathways and cancer-relevant targets (Fig. 6*A*). Thereby these results provide functional validation of global impact of PP2A on pathway functions. Consistently with previous results implicating PP2A inhibition as a drug resistance mechanism (5, 8, 14, 16, 30), PPP2R1A depletion increased average drug resistance across all 238 drugs (Fig. 6, *A* and *B*). On the other hand, the most potent induction of protein dephosphorylation by SET depletion (Fig. S1*H*) correlated with sensitization of cells to all the drugs on average (Fig. 6, *A* and *B*). Consistent with the weaker influence of CIP2A and PME-1 on phosphoproteome as compared with SET (Fig. S1*H*), their effects on the drug sensitivities were in many cases similar to that of SET, albeit of lower magnitudes (Fig. 6*A*). The most evident correlation between overall dephosphorylation activity and drug response was observed with aurora kinase (AURK) inhibitors ($p = 0.0057$ for enrichment) and JAK2 inhibitors ($p = 0.0142$) (Fig. 6, *A*, *C*, and *D*). PPP2R1A inhibition induced resistance to these drugs, whereas increased dephosphorylation potentiated the drug effects. Consistently, small molecule PP2A activator DT-061 potentiated the effects of the AURK inhibitor barasertib in HeLa and MV4-11 AML cells (Fig. S7*A*). In line with the broad impact of PP2A modulations on kinase pathway activities (Fig. 4, *D* and *E*), PPP2R1A depletion induced resistance also to broad selectivity kinase inhibitor midostaurin, whereas PME-1 and SET depletion increased sensitivity to this staurosporin derivative (Fig. S7*B*). Dephosphorylation activity also correlated with response to four HSP90 inhibitors with a pattern that was consistent with kinase inhibitor responses (Fig. S7*C*). This is likely to be related to HSP90 function as a chaperone for a majority of human kinome (60). Reassuringly, PP2A modulations were shown to impact heat-response processes in the pathway analysis (Fig. 3*A* and Fig. S5), providing a link between these two systematic PP2A modulation analyses. Furthermore, consistent with the prominent association of PP2A modulations with DNA and RNA synthesis pathways (Fig. 3*A* and Fig. S5), specific drug interactions were observed between PP2A modulations and several nucleoside synthesis inhibitors such as

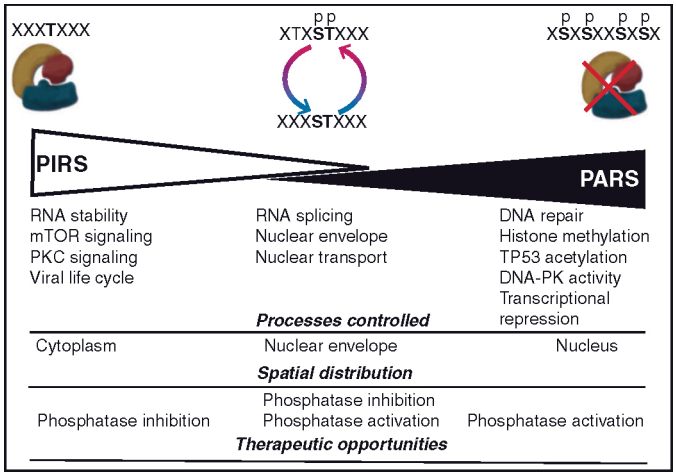


**Figure 7. Summary scheme of phosphoregulation rules by PP2A modulations.** Based on the results, most phosphosites and cellular processes appear to be sensitive to either phosphatase inhibition or activation. In contrast, only few processes show characteristics of bidirectional regulation. The preferable amino acid context for PIRS and PARS sites is also depicted. PIRS and PARS processes show differential spatial distribution between the cytoplasm and nucleus. Based on these results, efficient pharmacological interference with different cellular processes requires understanding whether those processes are either under PIRS or PARS dominance. As an example, phosphatase activation would mostly affect nuclear processes, whereas cytoplasmic processes would be most amenable to modulation by phosphatase inhibition.

dactinomycin, plicamycin, pemetrexed, cytarabine, and gemcitabine (Fig. S7*D*).

We found that certain drug responses were modulated only by PPP2R1A inhibition, similarly to its effects on the cellular processes observed above. Induction of resistance by PPP2R1A inhibition was observed for HDAC and bromodomain and extraterminal domain (BET) bromodomain inhibitors, while no sensitization effect with inhibition of any of the PAIPs was seen (Fig. 6, *E* and *F*). Notably, targets of these drugs, chromatin remodeling factors, were strongly enriched in PP2A-modulated targets, linking findings from the drug screen to cellular processes affected by PP2A modulations at the phosphoproteome level (Fig. 3*A* and Fig. S5). Moreover, the BET inhibitor results are consistent with the recently reported role of PP2A inhibition in JQ1 resistance in triple-negative breast cancer (61). Another interesting but atypical dependence was observed with mTOR that exhibited synergy with PPP2R1A inhibition, in contrast to the majority of drugs we screened (Fig. 6*G*). The observed sensitization to mTOR inhibitors may reflect an acquired dependence on increased mTOR activity in PPP2R1A-depleted cells, consistent with the up-regulation of PI3K/AKT/mTOR signaling in PPP2R1A-inhibited cells (16). The role of SET in mTOR inhibitor response was particularly interesting because only ATP-competitive mTOR inhibitors exhibited sensitization upon SET depletion (Fig. 6*G*). This sensitization to kinase inhibitor by SET inhibition can again be explained by phosphoproteomics results, as SET depletion was surprisingly found to activate PI3K/AKT/mTOR signaling (Fig. S7*E*).

Altogether, these data provide a systematic functional validation for impact of PP2A modulations on a wide range of cellular pathways and processes. In addition, these findings provide a knowledge resource for the development of combination strategies with the emerging PP2A-targeted therapies aiming either to reactivate (17, 18) or inhibit (62) PP2A (Fig. 7). This is particularly appealing as synergy between different drug families and pharmacological PP2A modulations has been recently established (16, 63).

## Discussion

Despite the essential importance of PP2A for growth and development, and for the pathogenesis of many diseases, our current understanding of the PP2A at the phosphoproteome level remains limited. Here, we characterized global phosphoproteome changes in PP2A-modulated cancer cells by inhibition of the structural PP2A scaffold protein PPP2R1A and three distinct endogenous PP2A-modulating proteins, the functions of which in cancer can be rescued by concomitant PP2A inhibition. Importantly, in addition to specific information related to pathways and processes, our data reveal generally relevant insights into the regulation of serine/threonine phosphorylation. Our biological insights are not only important for understanding cellular phosphosignaling, but also enable translational pharmacological studies to precisely modulate PP2A activity for single and combination therapies in cancer.

In addition to discovering a role for PP2A in a number of cancer-related processes, such as RNA processing (48, 49), one of our key discoveries is the differential dominance of either PPP2R1A or PAIP inhibition in the regulation of phosphosites, proteins, and cellular processes (Fig. 7). Although in our study the phosphorylation stoichiometry analysis (Fig. 2*A* and Fig. S2) was restricted only to a fraction of observed phosphopeptides, our results are in line with previous reports of global bimodal distribution between dephosphorylated and phosphorylated peptides (1, 42). The observed differential amino acid context of peptides regulated either by PP2A inhibition or reactivation is also consistent with previously reported preferential amino acid contexts of phosphosites regulated by kinases and phosphatases (40, 41, 43, 44). Appreciation of different phosphosites differentially regulated by phosphatase inhibition or activation may have in the future pharmacological relevance in predicting the outcomes of pharmacological PP2A targeting (17, 18, 62). Based on our results, basophilic targets would have a higher probability of responding to pharmacological PP2A inhibition, whereas PP2A reactivation therapies would primarily affect acidophilic target sites (Fig. 7). Our data also imply that the effects of pharmacological phosphatase reactivation cannot be directly deconvoluted from existing kinase inhibitor data. In a simplified model, phosphatase reactivation therapies would primarily affect sites occupied with phosphate, while kinase inhibition would not affect those sites that are already occupied with phosphate. Proof of principle for this model was recently shown in KRAS-mutant lung cancer cells in which PP2A inhibition up-regulated a different set of ERK targets than those that were inhibited by the MEK inhibitor (16).

One of the key unanswered question addressed in this study was (non)redundancy of PAIPs in regulation of cellular phosphoproteome. Previous reports (8, 10, 11, 15, 20, 22, 23, 27, 30–32) have identified several different functions regulated by CIP2A, PME-1, and SET, but thus far there has not been a systemic analysis of the degree of redundancy in the cellular

functions they regulate. At the global level, our data demonstrate that among these three PAIPs, SET has the most profound effects on cellular phosphoproteome (Fig. S1, *H* and *I*). The overlapping targets regulated by all of the PAIPs can be explained by direct inhibition of catalytic activity of PP2AC by both SET (27) and PME-1 (24), whereby they would also regulate the CIP2A-targeted PP2A complexes that, by current understanding, are restricted to B56-containing PP2A complexes (26). The nonoverlapping phosphoproteomes of CIP2A and PME-1 can instead be explained by the enzymatic activity of PME-1 as PP2AC C-terminal methylesterase and the role of methylation in promoting B55 subunit binding to PP2A complex (23, 39). Functionally differential roles for CIP2A and PME-1 were previously shown to be relevant for staurosporin resistance of glioblastoma cells that was driven by PME-1–mediated PP2A inhibition, but was not sensitive to CIP2A modulation (30). These conclusions were confirmed by drug screening in this study that demonstrated sensitization of cells to the staurosporin derivative midostaurin by depletion of PME-1 and SET, but not CIP2A (Fig. S7*B*). Our data also implicate that nuclear PP2A-modulating proteins may be a far-more important function in chromatin biology than previously appreciated. This could particularly be true for SET, as it associates with histones as a member of the INHAT complex with two other proteins (ANP32A and ANP32E) that also possess PP2A inhibitory activity (28, 65, 66). In conjunction with the different spatial distribution of PIRS and PARS targets discovered here, and the role of PAIPs in setting this balance (Fig. 5), we envision that SET-mediated PP2A inhibition at chromatin facilitates spatially restricted inhibition of dephosphorylation of chromatin remodeling complexes. Consequently, SET modulation by emerging small molecule approaches (67) could provide novel opportunities for targeting chromatin remodeling and epigenetic complexes for cancer therapy. Mechanistically, the widespread and coordinated dephosphorylation of protein complex components by PP2A may be explained by the recently characterized focal points of PP2A dephosphorylation activity that are facilitated by docking of PP2A to specific target proteins inside multiprotein complexes (44, 68, 69).

This study extended the recently demonstrated widespread dependence of kinase inhibitor responses on PP2A activity (16) across drug classes with diverse mechanisms of action. Besides insights to the design of combinatorial therapies with PP2A-modulating compounds (14, 33), our data may also facilitate novel patient therapy stratification strategies based on PPP2R1A mutations (21) or the expression of PAIPs (4) in patient tumors. In support of that, PME1-negative glioma cells were previously found to be hypersensitive to indolocarbazole kinase inhibitors *in vitro* and *in vivo* (30), and CIP2A positivity in chronic myeloid cells is a strong predictor of first generation tyrosine kinase inhibitor resistance (8). The current data with phosphoproteome profiles of cells with long-term suppression of either PP2A or PAIPs may thus help identify novel predictive phosphoprotein biomarkers and provide mechanistic explanations for the observed drug hypersensitivities.

In summary, this study provides the largest currently available resource for understanding the target processes affected by modulation of the major serine/threonine phosphatase PP2A. This systematic analysis of the biological redundancy and downstream targets of human PAIPs (CIP2A, PME-1, and SET) also provides the unbiased view on processes that would be most affected by targeting of these oncogenic proteins. We also provide an important resource for understanding how PP2A modulations impact cellular responses across a wide range of drugs and pathway inhibitors. Therapeutic modulation of PP2A has become realistic recently (17, 33, 62). Therefore, we anticipate that applying our datasets in the development of novel therapeutic agents may enable strategies of precision medicine for multiple human diseases (14).

## Experimental procedures

### *Cell culture and transfection*

HeLa, MDA–MB-231, PC-3, and MV4-11 cells were obtained from ATCC and cultured in Dulbecco's modified Eagle's medium (HeLa and MDA–MB-231) or RPMI (MV4-11) containing 10% fetal bovine serum, 2 mM glutamine, 50 IU/ml penicillin, and 50 $\mu$g/ml streptomycin. The cells were transfected with Oligofectamine (250 nM siRNA) according to the manufacturer's protocol (Life Technologies, Inc.). CIP2A was targeted with four siRNAs and the other genes with three siRNAs. Knockdown was validated by Western blotting and RT-quantitative PCR. siRNA sequences are presented in Table S4. PME-1 targeting by Crispr/Cas9 in PC-3 cells has been described in Ref. 70.

### *Phosphoproteomics*

Sample preparation, LC-MS/MS analysis, and the pairwise normalization for label-free quantitative phosphoproteomics were performed according to the previously published protocol (36). For RNAi, one million cells were plated on a 10-cm dish the day before transfection. siRNAs were transfected in a 7.5-ml volume using Oligofectamine and following the manufacturer's protocol. Each siRNA treatment was performed in triplicate for HeLa cells for a total of 9 (PPP2R1A, SET, and PME-1) or 12 (CIP2A) replicate samples per gene. Samples were collected 72 h after the transfection prior to reaching full confluency. Briefly, cells were washed once with ice-cold PBS, scraped into ice-cold PBS, and pelleted in a pre-cooled centrifuge. The pellets were snap-frozen and stored at −80 °C for later processing. Following steps were performed on ice or at 4 °C. Cells were lysed with buffer containing 50 mM Tris, pH 7.5, 8 M urea, 2 mM EGTA, 5 mM EDTA, 30 mM sodium fluoride, 60 mM $\beta$-glycerophosphate, 20 mM sodium pyrophosphate, 1 mM sodium orthovanadate, 5 $\mu$M pepstatin A, and a Complete protease inhibitor mixture tablet (Roche Applied Science). Lysates were sonicated with Bioruptor (Diagenode) at high intensity for 5 min with 15-s intervals and centrifuged for 35 min at 100,000 × *g*. Protein concentration of the supernatant was determined by measuring the absorbance at 280 nm

All phosphoproteomics sample preparation and LC-MS/MS analysis were performed at Turku Proteomics Facility according to Ref. 36, with some modifications (refer to Fig. S1*C*). Briefly, the cell lysates (1 mg protein) were mixed with a phosphoprotein standard bovine $\alpha$-casein (10 $\mu$g, Sigma), reduced with DTT, alkylated with iodoacetamide, and then digested with trypsin (Promega). After acidification with trifluoroacetic

acid (TFA), the samples were stored at −20 °C overnight or longer. Aliquots of the digests (10 of 1000 μl) were desalted with a microcolumn packed with Empore C18 disk (3M). For LC-MS/MS analysis, the samples (nonenriched digests) were reconstituted in 50 μl of 0.1% formic acid (FA), of which 6 μl was transferred into an LC sample vial for a 5-μl injection. The remaining digests (990 μl) were desalted with an Empore C18-SD 10-mm/6-ml cartridge (3M), followed by phosphopeptide enrichment with a microcolumn packed with Sachtopore-NP $TiO_2$ beads (20 μm, 300 Å; ZirChrom). The enriched phosphopeptides were immediately desalted with the C18 microcolumn. For LC-MS/MS analysis, the samples ($TiO_2$-enriched phosphopeptides) were reconstituted in 11 μl of 0.1% FA, of which 5.5 μl was transferred into an LC sample vial for a 5-μl injection.

LC-MS/MS analysis was performed using an EASY-nLC 1000 nanoflow LC instrument coupled to a Q Exactive quadrupole-orbitrap mass spectrometer (Thermo Fisher Scientific). A 100-μm × 2-cm trap column and a 75-μm × 15-cm analytical column were packed in-house with Magic C18AQ resin (200 Å, 5 μm; Michrom Bioresources). The mobile phases were 2% ACN, 0.2% FA (A) and 95% ACN, 0.2% FA (B). LC gradient elution condition was initially 2% B to 20% B (70 min), 40% B (100 min), and 100% B (105–110 min), with a flow rate of 300 nl/min. Data-dependent acquisition was performed in positive ion mode. For the first set of the samples, MS spectra were acquired from $m/z$ 300 to $m/z$ 2000 with a resolution of 70,000 at $m/z$ 200, a target value of 1,000,000 ions, and a maximal injection time of 120 ms, in profile mode. The 10 most abundant ions of which charge states were 2+ or higher were selected for subsequent fragmentation (higher-energy collisional dissociation) with a normalized collision energy of 30, and MS/MS spectra were acquired with a resolution of 17,500 at $m/z$ 200, a target value of 50,000 ions, a maximal injection time of 250 ms, and the lowest mass fixed at $m/z$ 100, in profile mode. Dynamic exclusion duration was 30 s. The lock-mass option was used ($m/z$ 445.12003). For the second set of the samples, some conditions were modified, as MS acquisition was performed with a resolution of 140,000, a target value of 3,000,000 ions, and a maximal injection time of 100 ms, and MS/MS acquisition was in centroid mode.

After LC-MS/MS analysis of the $TiO_2$-enriched samples, the samples remaining in the vials (<0.5 μl each) were collected into nine mixtures and subjected to enzymatic dephosphorylation with calf intestinal alkaline phosphatase (Roche Applied Science). After acidification with FA and desalting with the C18 microcolumn, the dephosphorylated samples were reconstituted in 5.5 μl of 0.1% FA, of which 5 μl was loaded to LC-MS/MS.

Phosphopeptide identification was performed according to Ref. 36 with some modifications (see Fig. S1*C*). LC-MS/MS data of the $TiO_2$-enriched and -nonenriched samples were searched with Mascot (version 2.4.1) via Proteome Discoverer (version 1.4.1.14, Thermo Fisher Scientific), against a concatenated forward-reverse SwissProt database (v2012_04, *Homo sapiens*) supplemented with common contaminants (20,339 protein sequences and 20,339 decoys). The search criteria were as follows: trypsin as an enzyme; two missed cleavage sites allowed; carbamidomethylation of cysteine as a fixed modification; oxidation of methionine and phosphorylation of serine/threonine/tyrosine and acetylation of the protein N terminus as variable modifications; peptide mass tolerance of 5 ppm; and MS/MS ion tolerance of 0.02 Da. For phosphorylation site localization, phospho-RS (version 3.0, the neutral loss option disabled) was enabled. In parallel, peak lists (mgf files) for the $TiO_2$-enriched samples were exported.

MS/MS spectra of all possible isoforms of singly phosphorylated peptides were simulated using SimPhospho program based on MS/MS identification of the dephosphorylated peptides (71). As the dephosphorylated peptides, nine LC-MS/MS data acquired in this study and two LC-MS/MS data previously reported (71) were used. Dephosphorylated peptides were searched with Mascot, where PeptideProphet probability of ≥0.95, Mascot expectation value of ≤0.05, and Δ score of ≥10 were applied as a cutoff. After the phosphorylation simulation, a consensus spectral library (SimHeLa) was built using SpectraST (version 4.0, released beta), which consists of 21,922 spectra for 4774 peptide sequences. SpectraST searching against the SimHeLa library (SimSpectraST searching (71)) was performed for the $TiO_2$-enriched samples via Proteome Discoverer by submitting the mgf files. The SwissProt database without the reversed sequences was used, and peptide mass tolerance was set to 3 Da. Percolator was enabled for estimating probability. The search was repeated against the library supplemented with decoy entries, using the stand-alone SpectraST (after adjusting the mgf file format) to obtain its *F*-value and recalculated ΔDot score that are required for phosphorylation site localization.

All the Mascot and SimSpectraST results were merged on Proteome Discoverer. An xlsx file was exported after applying a Mascot expectation value of ≤0.05, Percolator PEP of ≤0.05, minimum 7 amino acid length, search engine rank 1, and protein grouping. As cutoffs for 1% false localization rate (*i.e.* high-confidence phosphorylation sites), phospho-RS probability of ≥99.3% was used, while a SpectraST (standalone) *F*-value of ≥0.49 and a recalculated ΔDot score of ≥0.005 were applied only when a singly-phosphorylated peptide contained >1 Ser/Thr/Tyr in its sequence (71). Based on the localization confidence (high or low), a new score was given for each phosphopeptide spectral match. When Mascot and SimSpectraST searches disagreed on high-confidence phosphosites, those were considered as low confidence. The scoring scheme is summarized in Table S5. From the $TiO_2$-enriched samples, 11,759 unique phosphopeptides were identified, at a false discovery rate of 0.11% estimated using the target-decoy strategy at a phosphopeptide spectral match level, *i.e.* 2× decoy matches/total matches.

Label-free quantification was performed using Progenesis LC-MS (version 4.1). The $TiO_2$-enriched and -nonenriched samples were processed separately. All the chromatographic data were aligned automatically and further adjusted manually. Peptide ion features were detected in the automatic mode with the highest sensitivity. The features were assigned by importing the xlsx identification file, followed by applying a 5-ppm mass tolerance filter. All the features assigned to human peptides were used for global median centering of abundance ratios.

Protein abundance was quantified based on the sum of ion abundances of peptides unique to a protein. After annotating phosphorylation sites on proteins, the abundance of phosphosites was quantified based on the sum of ion abundances of phosphopeptide variants (*i.e.* different charge, missed cleavage, oxidation, and/or acetylation states). When a phosphosite was assigned to both high and low localization confidence features, only the former was taken into account.

The directionality of regulation by PPP2R1A and PAIPs in the HeLa samples was robust to the selection of normalization method (Fig. 1*C* and Fig. S7*F*); however, we observed positive skewing of the fold change distribution by PPP2R1A depletion and negative skewing by depletion of PAIPs (Fig. 1*C* and Fig. S7*F*). This is likely a result of up-regulation and down-regulation, respectively, of a significant fraction of phosphosites in these samples (Fig. 1*C*) and supports the selection of pairwise normalization as described in Ref. 36. The directionality of regulation was also consistent across different siRNAs (Fig. S1*D*). The HeLa cell data consist of two sets analyzed at different times, and the peptides displaying the batch effect were filtered out. Specifically, linear regression model residuals in phosphopeptide sample triplicate abundances displayed bimodality after imputing the smallest nonzero values for nondetected abundances, coupled with log2-transformation, and the phosphopeptides displaying high variance were filtered out before downstream analysis. The differential expression of the filtered dataset was then examined using the popular variance-pooling linear regression R-package limma (72), where each case triplicate was compared with the corresponding scrambled control triplicate

### *Statistics*

Statistical analyses were performed using JMP Pro (version 12.0 for Windows software, SAS Institute Inc.), Graphpad PRISM (version 6, Graphpad Software Inc.), and R (RRID: SCR_001905). Continuous variables were compared using the *t* test and limma. False discovery rate of limma was controlled by Storey procedure (*q* value). All the statistical tests were two-sided and considered significant at $p \leq 0.05$. When necessary for the assumption of normal distribution, log transformations were performed for continuous variables. For categorical data, frequencies were compared using the $\chi^2$ test.

### *Soft clustering, pathway analyses, and motif enrichment*

Soft clustering was performed in R using Mfuzz package (73). After obtaining similar results with a range of different cluster size and fuzzification parameters, we selected the parameters c = 6 and m = 2 for the analysis similarly to Olsen *et al.* (74). Soft clustering was also performed on a previously released dataset on A549 cells (ProteomeXchange accession number: PXD009900). Sample preparation for these data has been described previously (16), and data were analyzed similarly to HeLa cell data. Pathway enrichment analysis was performed using the g:Profiler R package (46). We selected biological processes of Gene Ontology and molecular pathways of Reactome as data sources for pathway analysis. We used the default method of multiple testing correction and filtered results by corrected significance cutoff of $q < 0.05$. We also limited gene sets to include between 3 and 500 genes. The background list for pathway enrichment analyses included the unique list of all proteins from our dataset combined with all known human phosphoproteins. The phosphoproteins were retrieved from the PhosphoSitePlus database (75) and were filtered to include previously published results ("MS_LIT" and "LT_LIT"). Protein names in the background set were converted to gene IDs of the Ensembl database using the g:Convert feature of g:Profiler. This procedure provided a list of enriched pathways for each condition. The lists were merged into a unified pathway-condition table and visualized with the Enrichment Map app (76) in Cytoscape (77). Finally, we manually reviewed the Enrichment Map and grouped into the most representative functional themes.

The following filtering steps were performed for pathway enrichment analysis. First, a list of unique proteins was constructed by selecting the peptide with the lowest *p* value for every protein. Second, unique proteins were filtered using a corrected *p* value cutoff ($q \leq 0.05$). Third, the final list of proteins was ranked by the significance (*p* value) for subsequent pathway enrichment analysis. Analysis of phosphopeptide clusters was carried out similarly. Clusters were compiled by assigning proteins to clusters based on maximum probability. For proteins with multiple identified peptides, we selected the peptide with highest cluster membership (Table S1) to represent the protein and thus obtained nonredundant lists of unique proteins. The final lists of proteins were ranked according to the cluster membership probabilities.

Enrichment of canonical pathway components in the clusters, as well as subcellular localization of the proteins, was analyzed with Ingenuity Pathway Analysis, Spring 2015 release version (Qiagen). Kinase target predictions were performed with NetworKIN and NetPhorest (78). Enriched phosphosite motifs were analyzed with motif-x (79). The GO term enrichments shown in Fig. 3*B* were obtained by STRING database (version 11) (80) using significantly regulated peptides ($q < 0.05$) from Table S1.

### *Drug-sensitivity testing*

For the high-throughput DSRT analyses, cells were transfected 3 days prior to plating them on the drug-containing 384-well plates at a confluency of 1000 cells/well. The subsequent analyses were carried out as described previously (58). Analysis was repeated with three (PPP2R1A, SET, and PME-1) or four (CIP2A) different siRNAs for each gene. The ΔDSS (59) was calculated by comparing the response of each siRNA-depleted sample to the average of three control samples. In cell-viability experiments with Barasertib (Sigma) and DT-061 (MedChemExpress, HY-112929), 5000 (HeLa) or 50,000 (MV4-11) cells per well were plated on 96-well plates and cultured for 3 days in the presence of drugs and measured with WST1 assay according to the manufacturer's recommendation (Roche Applied Science). After 3 days of culture, cells were incubated for 30 min with WST1 reagent, shaken at 250 rpm for 2 min, and followed by measurement of absorbance at 440 nm. Five independent experiments were performed for both cell lines.

In Western blot assays for PP2A target validation, indicated cell types were seeded on either 6-well plates or 10-cm dishes 24 h prior to drug treatment. Cells were treated for the indi-

cated times with either 25 nM concentration of okadaic acid (LC Labs, O-6410), 10 $\mu$M concentration of FTY-720 (Selleckchem, S5002), 5 and 10 $\mu$M DT-061 (MedChemExpress, HY-112929), or 0.1–10 $\mu$M RO-3306.

### *Enrichment of drug groups*

The numbers of up-regulated phosphopeptides for each gene were subtracted from the number of down-regulated phosphopeptides, and the difference values were used as a PP2A activity index. Uncentered Pearson's correlation coefficients were calculated between the PP2A activity index and DSS drug response values for each drug. Drugs were then ranked by correlation with PP2A activity index. Enrichment scores for selected drug groups in the ranked lists were calculated similarly to Gene Set Enrichment Analysis (64).

### *Cell stainings*

For proximity ligation assay, cells were plated on coverslips 2 days after transfection. On the following day, subconfluent cells were fixed with 3:1 acetone methanol in −20 °C for 10 min, and proximity ligation assay was performed with Duolink kit (Sigma) according to the manufacturer's protocol. Briefly, cells were blocked with blocking solution and incubated in a preheated humidity chamber for 30 min at 37 °C, followed by incubation with primary antibodies (PPP2R1A, sc-15355, Santa Cruz Biotechnology; Lamin A/C, sc-6215, Santa Cruz Biotechnology) overnight at 4 °C. After the last wash, slides were mounted with Mowiol mounting medium and imaged on an LSM780 confocal microscope (Carl Zeiss). To study the mitotic fraction of PP2A-modulated HeLa cells, the cells were transfected in six-well plates, and 48 h later 20,000 cells were reseeded in chambered ibiTreat $\mu$-Slide coverslip, which has a hydrophilic surface for optimal cell adhesion (80826, Ibidi). 24 h later cells were fixed using 4% paraformaldehyde (prewarmed at 37 °C) for 15 min at room temperature. Permeabilization was done using 1% Triton X-100 (Sigma) in PBS at room temperature for 15 min, and cells were blocked in 10% goat serum (ab7481, Abcam) in PBS for 30 min at room temperature. For visualizing serine 10-phosphorylated histones, cell were incubated overnight at 4 °C in rabbit phospho-H3 (Millipore, 06-570) antibody diluted to 1:500 in 10% goat serum. Cells were washed three times in PBS and incubated in secondary antibody, Alexa Fluor 488 goat anti-rabbit IgG (A-11008, Invitrogen) diluted to 1:1000 in 10% goat serum for 1 h at room temperature, and then in 4,6-diamidino-2-phenylindole (D1306, Invitrogen) for 10 min at room temperature. Cells were imaged using confocal microscope (3i CSU-W1 spinning disk) and quantified by software FIJI. Mitotic index was calculated as a percentage of histone positive cells to the total number of cells.

### *Western blotting*

For Western blot analysis, the following standard protocol was used with minor occasional modifications. Cells were harvested by scraping in ice-cold PBS and lysed in RIPA buffer (50 mM Tris-HCl, pH 7.5, 0.5% deoxycholate, 0.1% SDS, 1% Nonidet P-40, and 150 mM NaCl) with protease and phosphatase inhibitors (4693159001 and 4906837001, Roche Applied Science). Lysates were sonicated using Bioruptor sonicator (Diagenode) and centrifuged at full speed for 20 min. Supernatant was collected, and protein concentration was determined using Pierce™ BCA protein assay kit (Thermo Fisher Scientific, 23227). 10–20 $\mu$g of protein sample was boiled in 6× loading buffer and resolved on 4–20% precast protein gels (456-1093 and 456-1096, Bio-Rad). Separated proteins were blotted on a PVDF membrane using Trans-Blot® Turbo™ Transfer System (170-4155) by Bio-Rad. PVDF membrane was blocked in 5% milk/TBS/Tween for 1 h at room temperature and then incubated with primary antibodies 2 h to overnight at 4 °C. After washing, the membrane was incubated in secondary antibody for 1 h at room temperature and developed by ECL Western blotting substrate (32106, Pierce). The following antibodies were used: CIP2A, sc-80659 (Santa Cruz Biotechnology); GAPDH, 5G4–6C5 (HyTest Ltd.); PME1, sc-20086 (Santa Cruz Biotechnology); PPP2R1A, sc-15355 (Santa Cruz Biotechnology); SET, sc-133138 (Santa Cruz Biotechnology); p-Lamin S22, no. 2016 (Cell Signaling Technology); Lamin A/C, sc-6215 (Santa Cruz Biotechnology); anti-phospho-DNMT1(Ser-714): 07-1594, EMD Millipore, Merck (1:250); anti-SET (F-9): sc-133138, Santa Cruz Biotechnology (1:500–1000); anti-$\beta$-actin: A1978, Sigma (1:5000); phospho-Ser-2–Max (Biorbyt, orb335746); phospho-Ser-394–HDAC2 (Thermo Fisher Scientific, PA5–35395); GAPDH (5G4–6C5, HyTest Ltd.). The antibody for p-vimentin was a generous gift from Professor John Eriksson (Åbo Akademi University, Turku, Finland). For phospho-motif antibodies, we used phospho-(Ser/Thr) kinase substrate antibody sampler kit no. 9920 (Cell Signaling Technology) and phospho-CK2 substrate ((pS/pT)D*X*E) MultiMab™ rabbit mAb mix no. 8738 (Cell Signaling Technology). Secondary antibodies were purchased from Dako (P0447 and P0399). The densitometry analysis of blots was performed with ImageJ software.

### *Nucleophosmin mutants*

The following primer pairs were used to generate NPM-1 mutants, written in the 5′–3′ direction for forward and reverse primer, respectively: S254A, CAA GCA GCG ATA GAA AAA GGT GGT TCT CTT C and C TTT TTC TAT CGC TGC TTG CAT TTT TGC TTT AAT GTC; S260A, GGT GGT GCG CTT CCC AAA GTG GAA GCC AAA TTC and GGG AAG CGC ACC ACC TTT TTC TAT CGC TGC; S254D, CAA GCA GAT ATA GAA AAA GGT GGT TCT CTT C and C TTT TTC TAT ATC TGC TTG CAT TTT TGC TTT AAT GTC; S260D, GGT GGT GAT CTT CCC AAA GTG GAA GCC AAA TTC and GGG AAG ATC ACC ACC TTT TTC TAT CGC TGC. All constructs were generated by mutagenesis using PCR with Phusion Green Hot Start High-Fidelity PCR Master Mix (F-5665, Thermo Fisher Scientific) and DpnI enzyme from QuikChange Lightning site-directed mutagenesis kit (210518-5, Agilent Technologies). GFP-NPM-1 WT was from Addgene (17578). DH5$\alpha$ cells were routinely used for plasmid propagation. For DNA extraction and purification, the following commercial kits were used according to the manufacturer's instructions: NucleoSpin plasmid (740588.50) and NucleoBond Xtra Maxi Plus EF (740426.50, both from Biotop). Samples were verified by sequencing at FIMM (Helsinki, Finland). For cell transfection, the MDA–MB-231 cells were plated in a 12-well plate

format and transfected using Lipofectamine 2000 (Thermo Fisher Scientific). Per well, 1 $\mu$g of DNA and 3 $\mu$l of Lipofectamine 2000 were diluted in 100 $\mu$l of Opti-MEM while the cells were left in full growth medium. 24 h post-transfection, the cells were imaged using EVOS cell-imaging system, with a filter for GFP.

### *Data availability*

Raw MS data, protein sequence database, spectral libraries, and search results have been deposited to the jPOST repository with the data set identifier JPST000692 (ProteomeXchange identifier PXD016102).

*Author contributions*—O. K., S. Y. I., K. W., T. A., and J. W. conceptualization; O. K., S. Y. I., L. Y., T. D. L., T. A., and J. W. data curation; O. K., S. Y. I., E. K., L. Y., T. D. L., M. J., P. H., L. R., B. Y., J. R., T. A., and J. W. formal analysis; O. K. validation; O. K., S. Y. I., E. K., L. Y., M. S., K. P., A. A., C. R., B. Y., T. V., and J. W. investigation; O. K. and J. W. visualization; O. K., S. Y. I., T. D. L., and K. P. methodology; O. K. writing-original draft; O. K. and J. W. project administration; O. K. and J. W. writing-review and editing; L. Y., T. D. L., V. S., and T. A. software; G. L. C., J. R., K. W., T. A., and J. W. supervision; J. R. resources; J. W. funding acquisition.

*Acknowledgments—We thank a number of colleagues for their constructive advice and comments to different versions of this manuscript during its submission process to a number of scientific journals over past 3 years. The expert technical help of Taina Kalevo-Mattila is greatly acknowledged. We also thank professional help from Turku Proteomics Facility and Turku Bioscience Genome Editing Core both funded by Biocenter Finland.*

### References

1. Sharma, K., D'Souza, R. C., Tyanova, S., Schaab, C., Wiśniewski, J. R., Cox, J., and Mann, M. (2014) Ultradeep human phosphoproteome reveals a distinct regulatory nature of Tyr and Ser/Thr-based signaling. *Cell Rep.* **8,** 1583–1594 CrossRef Medline
2. Meeusen, B., and Janssens, V. (2018) Tumor suppressive protein phosphatases in human cancer: emerging targets for therapeutic intervention and tumor stratification. *Int. J. Biochem. Cell Biol.* **96,** 98–134 CrossRef Medline
3. Perrotti, D., and Neviani, P. (2013) Protein phosphatase 2A: a target for anticancer therapy. *Lancet Oncol.* **14,** e229–e238 CrossRef Medline
4. Kauko, O., and Westermarck, J. (2018) Non-genomic mechanisms of protein phosphatase 2A (PP2A) regulation in cancer. *Int. J. Biochem. Cell Biol.* **96,** 157–164 CrossRef Medline
5. Neviani, P., Santhanam, R., Trotta, R., Notari, M., Blaser, B. W., Liu, S., Mao, H., Chang, J. S., Galietta, A., Uttam, A., Roy, D. C., Valtieri, M., Bruner-Klisovic, R., Caligiuri, M. A., Bloomfield, C. D., *et al.* (2005) The tumor suppressor PP2A is functionally inactivated in blast crisis CML through the inhibitory activity of the BCR/ABL-regulated SET protein. *Cancer Cell* **8,** 355–368 CrossRef Medline
6. Hahn, W. C., Dessain, S. K., Brooks, M. W., King, J. E., Elenbaas, B., Sabatini, D. M., DeCaprio, J. A., and Weinberg, R. A. (2002) Enumeration of the simian virus 40 early region elements necessary for human cell transformation. *Mol. Cell. Biol.* **22,** 2111–2123 CrossRef Medline
7. Rangarajan, A., Hong, S. J., Gifford, A., and Weinberg, R. A. (2004) Species- and cell type-specific requirements for cellular transformation. *Cancer Cell* **6,** 171–183 CrossRef Medline
8. Lucas, C. M., Harris, R. J., Holcroft, A. K., Scott, L. J., Carmell, N., McDonald, E., Polydoros, F., and Clark, R. E. (2015) Second generation tyrosine kinase inhibitors prevent disease progression in high-risk (high CIP2A) chronic myeloid leukaemia patients. *Leukemia* **29,** 1514–1523 CrossRef Medline
9. Ruediger, R., Ruiz, J., and Walter, G. (2011) Human cancer-associated mutations in the A$\alpha$ subunit of protein phosphatase 2A increase lung cancer incidence in A$\alpha$ knockin and knockout mice. *Mol. Cell. Biol.* **31,** 3832–3844 CrossRef Medline
10. Junttila, M. R., Puustinen, P., Niemelä, M., Ahola, R., Arnold, H., Böttzauw, T., Ala-aho, R., Nielsen, C., Ivaska, J., Taya, Y., Lu, S. L., Lin, S., Chan, E. K., Wang, X. J., Grènman, R., *et al.* (2007) CIP2A inhibits PP2A in human malignancies. *Cell* **130,** 51–62 CrossRef Medline
11. Laine, A., Sihto, H., Come, C., Rosenfeldt, M. T., Zwolinska, A., Niemelä, M., Khanna, A., Chan, E. K., Kähäri, V. M., Kellokumpu-Lehtinen, P. L., Sansom, O. J., Evan, G. I., Junttila, M. R., Ryan, K. M., Marine, J. C., *et al.* (2013) Senescence sensitivity of breast cancer cells is defined by positive feedback loop between CIP2A and E2F1. *Cancer Discov.* **3,** 182–197 CrossRef Medline
12. Chen, W., Arroyo, J. D., Timmons, J. C., Possemato, R., and Hahn, W. C. (2005) Cancer-associated PP2A A$\alpha$ subunits induce functional haploinsufficiency and tumorigenicity. *Cancer Res.* **65,** 8183–8192 CrossRef Medline
13. Walter, G., and Ruediger, R. (2012) Mouse model for probing tumor suppressor activity of protein phosphatase 2A in diverse signaling pathways. *Cell Cycle* **11,** 451–459 CrossRef Medline
14. Westermarck, J. (2018) Targeted therapies don't work for a reason; the neglected tumor suppressor phosphatase PP2A strikes back. *FEBS J.* **285,** 4139–4145 CrossRef Medline
15. Richard, N. P., Pippa, R., Cleary, M. M., Puri, A., Tibbitts, D., Mahmood, S., Christensen, D. J., Jeng, S., McWeeney, S., Look, A. T., Chang, B. H., Tyner, J. W., Vitek, M. P., Odero, M. D., Sears, R., and Agarwal, A. (2016) Combined targeting of SET and tyrosine kinases provides an effective therapeutic approach in human T-cell acute lymphoblastic leukemia. *Oncotarget* **7,** 84214–84227 CrossRef Medline
16. Kauko, O., O'Connor, C. M., Kulesskiy, E., Sangodkar, J., Aakula, A., Izadmehr, S., Yetukuri, L., Yadav, B., Padzik, A., Laajala, T. D., Haapaniemi, P., Momeny, M., Varila, T., Ohlmeyer, M., Aittokallio, T., *et al.* (2018) PP2A inhibition is a druggable MEK inhibitor resistance mechanism in KRAS-mutant lung cancer cells. *Sci. Transl. Med.* **10,** eaaq1093 CrossRef Medline
17. Sangodkar, J., Perl, A., Tohme, R., Kiselar, J., Kastrinsky, D. B., Zaware, N., Izadmehr, S., Mazhar, S., Wiredja, D. D., O'Connor, C. M., Hoon, D., Dhawan, N. S., Schlatzer, D., Yao, S., Leonard, D., *et al.* (2017) Activation of tumor suppressor protein PP2A inhibits KRAS-driven tumor growth. *J. Clin. Invest.* **127,** 2081–2090 CrossRef Medline
18. O'Connor, C. M., Perl, A., Leonard, D., Sangodkar, J., and Narla, G. (2018) Therapeutic targeting of PP2A. *Int. J. Biochem. Cell Biol.* **96,** 182–193 CrossRef Medline
19. Merisaari, J., Denisova, O. V., Doroszko, M., Le Joncour, V., Johansson, P., Leenders, W. P. J., Kastrinsky, D. B., Zaware, Z., Narla, G., Laakkonen, P., Nelander, S., Ohlmeyer, M., and Westermarck, J. (2020) Monotherapy efficacy of BBB-permeable small molecule reactivators of PP2A in glioblastoma. *Brain Commun.* **2,** fcaa002 CrossRef
20. Shentu, Y. P., Huo, Y., Feng, X. L., Gilbert, J., Zhang, Q., Liuyang, Z. Y., Wang, X. L., Wang, G., Zhou, H., Wang, X. C., Wang, J. Z., Lu, Y. M., Westermarck, J., Man, H. Y., and Liu, R. (2018) CIP2A causes Tau/APP phosphorylation, synaptopathy, and memory deficits in Alzheimer's disease. *Cell Rep.* **24,** 713–723 CrossRef Medline
21. Taylor, S. E., O'Connor, C. M., Wang, Z., Shen, Q., Song, H., Leonard, D., Sangodkar, J., LaVasseur, C., Avril, S., Waggoner, S., Zanotti, K., Armstrong, A. J., Nagel, C., Resnick, K., Singh, S., Jackson, M. W., *et al.* (2019) The highly recurrent PP2A A$\alpha$-subunit mutation P179R alters protein structure and impairs PP2A enzyme function to promote endometrial tumorigenesis. *Cancer Res.* **79,** 4242–4257 CrossRef
22. Khanna, A., Pimanda, J. E., and Westermarck, J. (2013) Cancerous inhibitor of protein phosphatase 2A, an emerging human oncoprotein and a potential cancer therapy target. *Cancer Res.* **73,** 6548–6553 CrossRef Medline
23. Kaur, A., and Westermarck, J. (2016) Regulation of protein phosphatase 2A (PP2A) tumor suppressor function by PME-1. *Biochem. Soc. Trans.* **44,** 1683–1693 CrossRef Medline

24. Xing, Y., Li, Z., Chen, Y., Stock, J. B., Jeffrey, P. D., and Shi, Y. (2008) Structural mechanism of demethylation and inactivation of protein phosphatase 2A. *Cell* **133,** 154–163 CrossRef Medline
25. Muto, S., Senda, M., Akai, Y., Sato, L., Suzuki, T., Nagai, R., Senda, T., and Horikoshi, M. (2007) Relationship between the structure of SET/TAF-Iβ/INHAT and its histone chaperone activity. *Proc. Natl. Acad. Sci. U.S.A.* **104,** 4285–4290 CrossRef Medline
26. Wang, J., Okkeri, J., Pavic, K., Wang, Z., Kauko, O., Halonen, T., Sarek, G., Ojala, P. M., Rao, Z., Xu, W., and Westermarck, J. (2017) Oncoprotein CIP2A is stabilized via interaction with tumor suppressor PP2A/B56. *EMBO Rep.* **18,** 437–450 CrossRef Medline
27. Arnaud, L., Chen, S., Liu, F., Li, B., Khatoon, S., Grundke-Iqbal, I., and Iqbal, K. (2011) Mechanism of inhibition of PP2A activity and abnormal hyperphosphorylation of tau by I2(PP2A)/SET. *FEBS Lett.* **585,** 2653–2659 CrossRef Medline
28. Li, M., Guo, H., and Damuni, Z. (1995) Purification and characterization of two potent heat-stable protein inhibitors of protein phosphatase 2A from bovine kidney. *Biochemistry* **34,** 1988–1996 CrossRef Medline
29. Niemelä, M., Kauko, O., Sihto, H., Mpindi, J. P., Nicorici, D., Pernilä, P., Kallioniemi, O. P., Joensuu, H., Hautaniemi, S., and Westermarck, J. (2012) CIP2A signature reveals the MYC dependency of CIP2A-regulated phenotypes and its clinical association with breast cancer subtypes. *Oncogene* **31,** 4266–4278 CrossRef Medline
30. Kaur, A., Denisova, O. V., Qiao, X., Jumppanen, M., Peuhu, E., Ahmed, S. U., Raheem, O., Haapasalo, H., Eriksson, J., Chalmers, A. J., Laakkonen, P., and Westermarck, J. (2016) PP2A inhibitor PME-1 drives kinase inhibitor resistance in Glioma cells. *Cancer Res.* **76,** 7001–7011 CrossRef Medline
31. Zhou, X., Updegraff, B. L., Guo, Y., Peyton, M., Girard, L., Larsen, J. E., Xie, X. J., Zhou, Y., Hwang, T. H., Xie, Y., Rodriguez-Canales, J., Villalobos, P., Behrens, C., Wistuba, I. I., Minna, J. D., and O'Donnell, K. A. (2017) PROTOCADHERIN 7 acts through SET and PP2A to potentiate MAPK signaling by EGFR and KRAS during lung tumorigenesis. *Cancer Res.* **77,** 187–197 CrossRef Medline
32. Jackson, J. B., and Pallas, D. C. (2012) Circumventing cellular control of PP2A by methylation promotes transformation in an Akt-dependent manner. *Neoplasia* **14,** 585–599 CrossRef Medline
33. Sangodkar, J., Farrington, C. C., McClinch, K., Galsky, M. D., Kastrinsky, D. B., and Narla, G. (2016) All roads lead to PP2A: exploiting the therapeutic potential of this phosphatase. *FEBS J.* **283,** 1004–1024 CrossRef Medline
34. Torrent, L., and Ferrer, I. (2012) PP2A and Alzheimer disease. *Curr. Alzheimer Res.* **9,** 248–256 CrossRef Medline
35. Sablina, A. A., Chen, W., Arroyo, J. D., Corral, L., Hector, M., Bulmer, S. E., DeCaprio, J. A., and Hahn, W. C. (2007) The tumor suppressor PP2A Aβ regulates the RalA GTPase. *Cell* **129,** 969–982 CrossRef Medline
36. Kauko, O., Laajala, T. D., Jumppanen, M., Hintsanen, P., Suni, V., Haapaniemi, P., Corthals, G., Aittokallio, T., Westermarck, J., and Imanishi, S. Y. (2015) Label-free quantitative phosphoproteomics with novel pairwise abundance normalization reveals synergistic RAS and CIP2A signaling. *Sci. Rep.* **5,** 13099 CrossRef Medline
37. Grallert, A., Boke, E., Hagting, A., Hodgson, B., Connolly, Y., Griffiths, J. R., Smith, D. L., Pines, J., and Hagan, I. M. (2015) A PP1-PP2A phosphatase relay controls mitotic progression. *Nature* **517,** 94–98 CrossRef Medline
38. Cordeiro, M. H., Smith, R. J., and Saurin, A. T. (2018) A fine balancing act: a delicate kinase-phosphatase equilibrium that protects against chromosomal instability and cancer. *Int. J. Biochem. Cell Biol.* **96,** 148–156 CrossRef Medline
39. Longin, S., Zwaenepoel, K., Louis, J. V., Dilworth, S., Goris, J., and Janssens, V. (2007) Selection of protein phosphatase 2A regulatory subunits is mediated by the C terminus of the catalytic subunit. *J. Biol. Chem.* **282,** 26971–26980 CrossRef Medline
40. Pinna, L. A., and Donella-Deana, A. (1994) Phosphorylated synthetic peptides as tools for studying protein phosphatases. *Biochim. Biophys. Acta* **1222,** 415–431 CrossRef Medline
41. Schweiger, R., and Linial, M. (2010) Cooperativity within proximal phosphorylation sites is revealed from large-scale proteomics data. *Biol. Direct* **5,** 6 CrossRef Medline
42. Wu, R., Haas, W., Dephoure, N., Huttlin, E. L., Zhai, B., Sowa, M. E., and Gygi, S. P. (2011) A large-scale method to measure absolute protein phosphorylation stoichiometries. *Nat. Methods* **8,** 677–683 CrossRef Medline
43. Pinna, L. A., and Ruzzene, M. (1996) How do protein kinases recognize their substrates? *Biochim. Biophys. Acta* **1314,** 191–225 CrossRef Medline
44. Hein, J. B., Hertz, E. P. T., Garvanska, D. H., Kruse, T., and Nilsson, J. (2017) Distinct kinetics of serine and threonine dephosphorylation are essential for mitosis. *Nat. Cell Biol.* **19,** 1433–1440 CrossRef Medline
45. Futschik, M. E., and Carlisle, B. (2005) Noise-robust soft clustering of gene expression time-course data. *J. Bioinform. Comput. Biol.* **3,** 965–988 CrossRef Medline
46. Reimand, J., Arak, T., Adler, P., Kolberg, L., Reisberg, S., Peterson, H., and Vilo, J. (2016) g:Profiler-a web server for functional interpretation of gene lists (2016 update). *Nucleic Acids Res.* **44,** W83–W89 CrossRef Medline
47. Dvinge, H., Kim, E., Abdel-Wahab, O., and Bradley, R. K. (2016) RNA splicing factors as oncoproteins and tumour suppressors. *Nat. Rev. Cancer* **16,** 413–430 CrossRef Medline
48. Obeng, E. A., Stewart, C., and Abdel-Wahab, O. (2019) Altered RNA processing in cancer pathogenesis and therapy. *Cancer Discov.* **9,** 1493–1510 CrossRef Medline
49. Box, J. K., Paquet, N., Adams, M. N., Boucher, D., Bolderson, E., O'Byrne, K. J., and Richard, D. J. (2016) Nucleophosmin: from structure and function to disease development. *BMC Mol. Biol.* **17,** 19 CrossRef Medline
50. Linding, R., Jensen, L. J., Pasculescu, A., Olhovsky, M., Colwill, K., Bork, P., Yaffe, M. B., and Pawson, T. (2008) NetworKIN: a resource for exploring cellular phosphorylation networks. *Nucleic Acids Res.* **36,** D695–D699 CrossRef Medline
51. Puustinen, P., Junttila, M. R., Vanhatupa, S., Sablina, A. A., Hector, M. E., Teittinen, K., Raheem, O., Ketola, K., Lin, S. Kast, J., Haapasalo, H., Hahn, W. C., and Westermarck, J. (2009) PME-1 protects extracellular signal-regulated kinase pathway activity from protein phosphatase 2A-mediated inactivation in human malignant Glioma. *Cancer Res.* **69,** 2870–2877 CrossRef Medline
52. Zheng, X. F., Kalev, P., and Chowdhury, D. (2015) Emerging role of protein phosphatases changes the landscape of phospho-signaling in DNA damage response. *DNA Repair* **32,** 58–65 CrossRef Medline
53. Ferrari, E., Bruhn, C., Peretti, M., Cassani, C., Carotenuto, W. V., Elgendy, M., Shubassi, G., Lucca, C., Bermejo, R., Varasi, M., Minucci, S., Longhese, M. P., and Foiani, M. (2017) PP2A controls genome integrity by integrating nutrient-sensing and metabolic pathways with the DNA damage response. *Mol. Cell* **67,** 266–281.e4 CrossRef Medline
54. Myant, K., Qiao, X., Halonen, T., Come, C., Laine, A., Janghorban, M., Partanen, J. I., Cassidy, J., Ogg, E. L., Cammareri, P., Laiterä, T., Okkeri, J., Klefström, J., Sears, R. C., Sansom, O. J., and Westermarck, J. (2015) Serine 62-phosphorylated MYC associates with nuclear lamins and its regulation by CIP2A is essential for regenerative proliferation. *Cell Rep.* **12,** 1019–1031 CrossRef Medline
55. Pokharel, Y. R., Saarela, J., Szwajda, A., Rupp, C., Rokka, A., Lal Kumar Karna, S., Teittinen, K., Corthals, G., Kallioniemi, O., Wennerberg, K., Aittokallio, T., and Westermarck, J. (2015) Relevance rank platform (RRP) for functional filtering of high content protein–protein interaction data. *Mol. Cell. Proteomics* **14,** 3274–3283 CrossRef Medline
56. Thul, P. J., Akesson, L., Wiking, M., Mahdessian, D., Geladaki, A., Ait Blal, H., Alm, T., Asplund, A., Bjork, L., Breckels, L. M., Backstrom, A., Danielsson, F., Fagerberg, L., Fall, J., Gatto, L., *et al.* (2017) A subcellular map of the human proteome. *Science* **356,** eaal3321 CrossRef Medline
57. Linding, R., Jensen, L. J., Ostheimer, G. J., van Vugt, M. A., Jørgensen, C., Miron, I. M., Diella, F., Colwill, K., Taylor, L., Elder, K., Metalnikov, P., Nguyen, V., Pasculescu, A., Jin, J., Park, J. G., *et al.* (2007) Systematic discovery of *in vivo* phosphorylation networks. *Cell* **129,** 1415–1426 CrossRef Medline
58. Pemovska, T., Kontro, M., Yadav, B., Edgren, H., Eldfors, S., Szwajda, A., Almusa, H., Bespalov, M. M., Ellonen, P., Elonen, E., Gjertsen, B. T., Karjalainen, R., Kulesskiy, E., Lagstrøm, S., Lehto, A., *et al.* (2013) Individualized systems medicine strategy to tailor treatments for patients with chemorefractory acute myeloid leukemia. *Cancer Discov.* **3,** 1416–1429 CrossRef Medline




ASBMB

59. Yadav, B., Pemovska, T., Szwajda, A., Kulesskiy, E., Kontro, M., Karjalainen, R., Majumder, M. M., Malani, D., Murumägi, A., Knowles, J., Porkka, K., Heckman, C., Kallioniemi, O., Wennerberg, K., and Aittokallio, T. (2014) Quantitative scoring of differential drug sensitivity for individually optimized anticancer therapies. *Sci. Rep.* **4,** 5193 CrossRef Medline
60. Taipale, M., Krykbaeva, I., Koeva, M., Kayatekin, C., Westover, K. D., Karras, G. I., and Lindquist, S. (2012) Quantitative analysis of HSP90-client interactions reveals principles of substrate recognition. *Cell* **150,** 987–1001 CrossRef Medline
61. Shu, S., Lin, C. Y., He, H. H., Witwicki, R. M., Tabassum, D. P., Roberts, J. M., Janiszewska, M., Huh, S. J., Liang, Y., Ryan, J., Doherty, E., Mohammed, H., Guo, H., Stover, D. G., Ekram, M. B., *et al.* (2016) Response and resistance to BET bromodomain inhibitors in triple-negative breast cancer. *Nature* **529,** 413–417 CrossRef Medline
62. Chung, V., Mansfield, A. S., Braiteh, F., Richards, D., Durivage, H., Ungerleider, R. S., Johnson, F., and Kovach, J. S. (2017) Safety, tolerability, and preliminary activity of LB-100, an inhibitor of protein phosphatase 2A, in patients with relapsed solid tumors. *Clin. Cancer Res.* **23,** 3277–3284 CrossRef Medline
63. Ho, W. S., Feldman, M. J., Maric, D., Amable, L., Hall, M. D., Feldman, G. M., Ray-Chaudhury, A., Lizak, M. J., Vera, J. C., Robison, R. A., Zhuang, Z., and Heiss, J. D. (2016) PP2A inhibition with LB100 enhances cisplatin cytotoxicity and overcomes cisplatin resistance in medulloblastoma cells. *Oncotarget* **7,** 12447–12463 CrossRef Medline
64. Subramanian, A., Tamayo, P., Mootha, V. K., Mukherjee, S., Ebert, B. L., Gillette, M. A., Paulovich, A., Pomeroy, S. L., Golub, T. R., Lander, E. S., and Mesirov, J. P. (2005) Gene set enrichment analysis: a knowledge-based approach for interpreting genome-wide expression profiles. *Proc. Natl. Acad. Sci. U.S.A.* **102,** 15545–15550 CrossRef Medline
65. Seo, S. B., McNamara, P., Heo, S., Turner, A., Lane, W. S., and Chakravarti, D. (2001) Regulation of histone acetylation and transcription by INHAT, a human cellular complex containing the set oncoprotein. *Cell* **104,** 119–130 CrossRef Medline
66. Costanzo, R. V., Vilá-Ortíz, G. J., Perandones, C., Carminatti, H., Matilla, A., and Radrizzani, M. (2006) Anp32e/Cpd1 regulates protein phosphatase 2A activity at synapses during synaptogenesis. *Eur. J. Neurosci.* **23,** 309–324 CrossRef Medline
67. Tibaldi, E., Pagano, M. A., Frezzato, F., Trimarco, V., Facco, M., Zagotto, G., Ribaudo, G., Pavan, V., Bordin, L., Visentin, A., Zonta, F., Semenzato, G., Brunati, A. M., and Trentin, L. (2017) Targeted activation of the SHP-1/PP2A signaling axis elicits apoptosis of chronic lymphocytic leukemia cells. *Haematologica* **102,** 1401–1412 CrossRef Medline
68. Afonso, O., Matos, I., Pereira, A. J., Aguiar, P., Lampson, M. A., and Maiato, H. (2014) Feedback control of chromosome separation by a midzone Aurora B gradient. *Science* **345,** 332–336 CrossRef Medline
69. Qian, J., Beullens, M., Lesage, B., and Bollen, M. (2013) Aurora B defines its own chromosomal targeting by opposing the recruitment of the phosphatase scaffold repo-man. *Curr. Biol.* **23,** 1136–1143 CrossRef Medline
70. Rupp, C., Aakula, A., Isomursu, A., Erickson, A., Kauko, O., Shah, P., Padzik, A., Kaur, A., Li, S. P., Pokharel, Y. R., Trotman, L., Rannikko, A., Taimen, P., Lammerding, J., Paatero, I., *et al.* (2019) PP2A inhibitor PME-1 suppresses anoikis, and is associated with therapy relapse of PTEN-deficient prostate cancers. *bioRxiv* CrossRef
71. Suni, V., Imanishi, S. Y., Maiolica, A., Aebersold, R., and Corthals, G. L. (2015) Confident site localization using a simulated phosphopeptide spectral library. *J. Proteome Res.* **14,** 2348–2359 CrossRef Medline
72. Ritchie, M. E., Phipson, B., Wu, D., Hu, Y., Law, C. W., Shi, W., and Smyth, G. K. (2015) limma powers differential expression analyses for RNA-sequencing and microarray studies. *Nucleic Acids Res.* **43,** e47 CrossRef Medline
73. Kumar, L., and E Futschik M. (2007) Mfuzz: a software package for soft clustering of microarray data. *Bioinformation* **2,** 5–7 CrossRef Medline
74. Olsen, J. V., Blagoev, B., Gnad, F., Macek, B., Kumar, C., Mortensen, P., and Mann, M. (2006) Global, *in vivo*, and site-specific phosphorylation dynamics in signaling networks. *Cell* **127,** 635–648 CrossRef Medline
75. Hornbeck, P. V., Zhang, B., Murray, B., Kornhauser, J. M., Latham, V., and Skrzypek, E. (2015) PhosphoSitePlus, 2014: mutations, PTMs and recalibrations. *Nucleic Acids Res.* **43,** D512–D520 CrossRef Medline
76. Merico, D., Isserlin, R., Stueker, O., Emili, A., and Bader, G. D. (2010) Enrichment map: a network-based method for gene-set enrichment visualization and interpretation. *PLoS ONE* **5,** e13984 CrossRef Medline
77. Shannon, P., Markiel, A., Ozier, O., Baliga, N. S., Wang, J. T., Ramage, D., Amin, N., Schwikowski, B., and Ideker, T. (2003) Cytoscape: a software environment for integrated models of biomolecular interaction networks. *Genome Res.* **13,** 2498–2504 CrossRef Medline
78. Horn, H., Schoof, E. M., Kim, J., Robin, X., Miller, M. L., Diella, F., Palma, A., Cesareni, G., Jensen, L. J., and Linding, R. (2014) KinomeXplorer: an integrated platform for kinome biology studies. *Nat. Methods* **11,** 603–604 CrossRef Medline
79. Chou, M. F., and Schwartz, D. (2011) Biological sequence motif discovery using motif-x. *Curr. Protoc. Bioinformatics 2011,* Chapter 13, Unit 13.15–24 CrossRef Medline
80. Szklarczyk, D., Gable, A. L., Lyon, D., Junge, A. Wyder, S., Huerta-Cepas, J, Simonovic, M., Doncheva, N. T., Morris, J. H., Bork, P, Jensen, L. J., and Mering, C. V. (2019) STRING version 11: protein–protein association networks with increased coverage, supporting functional discovery in genome-wide experimental datasets. *Nucleic Acids Res.* **47,** D607–D613 CrossRef Medline